JOURNAL OF PETROLOGY

Journal of Petrology, 2021, Vol. 62, No. 12, 1–25
doi: 10.1093/petrology/egab057
Advance Access Publication Date: 7 July 2021
Original Article

OXFORD

Warm and Slightly Reduced Mantle Under the Off-Rift Snæfellsnes Volcanic Zone, Iceland

Quinten H. A. van der Meer[1]*, Enikő Bali[1], Guðmundur H. Guðfinnsson[1], Maren Kahl [2] and Maja B. Rasmussen[1]

[1]Nordic Volcanological Center, Institute of Earth Sciences, University of Iceland, Sturlugata 7, 101 Reykjavík, Iceland; [2]Institut Für Geowissenchaften, Universität Heidelberg, Im Neuenheimer Feld 234-236, Heidelberg 69120, Germany

*Corresponding author. Present address: Nordic Volcanological Center, Institute of Earth Sciences, University of Iceland, Sturlugata 7, 101 Reykjavík, Iceland. E-mail: qvandermeer@gmail.com

Received 18 December 2020; Accepted 18 June 2021

ABSTRACT

Olivine (Fo_{75-91}) with spinel inclusions (Cr# 10–61) in basaltic lavas/tephras from the off-rift Snæfellsnes Volcanic Zone in Iceland record the chemistry, temperature and oxygen fugacity of fractionating magmas. After a detailed assessment of equilibrium conditions, crystallization temperatures and oxygen fugacity can be calculated from the composition of homogeneous Cr-spinel and Al-chromite inclusions in olivine phenocrysts. Geologically meaningful results can occasionally be obtained when homogenous spinel is enclosed in mildly zoned olivine and $K_D^{Mg\text{-}Fe}$ [$(Mg/Fe)_{olivine}/(Mg/Fe^{2+})_{spinel}$] is within the range for homogenous spinel in homogeneous olivine (3.5–4.3 for our samples). Spinel in normal zoned $Fo_{84.7–90.9}$ olivine records the primitive stages of magma fractionation and has crystallized from clinopyroxene-free primitive melts, probably at Moho depth and/or below. Discrepancies between $T_{ol\text{-}liq}$ ($Mg\text{-}Fe^{2+}$ diffusion sensitive) and T_{AL} (diffusion insensitive) suggest that some primitive olivines experienced magma mixing, completely overprinting their Fo content. Consequentially, $T_{ol\text{-}liq}$ in primitive olivines occasionally records residence rather than crystallization conditions. Temperature (1187–1317°C) gradually decreases across normal zoned $Fo_{84.7–90.9}$ olivine and controls fO_2 ($\Delta\log fO_2$ (QFM) -0.6 ± 0.2). Recharge-related primitive $Fo_{83.8–86.8}$ mantles of reverse zoned olivine contain the most primitive Cr-spinel linked to crustal magma storage zones. These spinels are mostly antecrysts with high Cr# (41.1–47.9) similar to spinel in normal zoned olivines that were captured by olivine and equilibrated in terms of $Mg\text{-}Fe^{2+}$. A rare olivine macrocryst crystallized alongside clinopyroxene (wehrlite) and includes abundant homogeneous Al-rich Cr-spinels. These are unique because they appear to record closed-system fractional crystallization rather than magma mixing and because they show that Cr-poor, Al-rich spinel crystallized alongside clinopyroxene. The macrocryst olivine–spinel pairs record lower crustal crystal mush conditions with fO_2 around the QFM buffer and $T_{ol\text{-}liq}$ of ~1200°C, similar to recharge-related mantles of reverse zoned olivine. More evolved compositions occur in the cores of reverse zoned olivine (Fo_{75-85}) that contain Cr-spinel, Fe-spinel and Al-magnetite. Contrary to spinel in more primitive olivine, these compositions are diverse and follow increasing $100Fe^{3+}/(Cr+Al+Fe^{3+})$ of 12.3 to 54.8 and TiO_2 (3.3 to 14.7 wt %) at decreasing Mg# (57.4 to 24.1) and Cr# (30.4 to 9.9) and rapidly increasing oxygen fugacities ($\Delta\log fO_2$ (QFM) +0.2 to +2.0) over only a limited temperature decrease ($T_{ol\text{-}liq}$: 1190 to 1145°C). These compositions span the 'spinel gap' and are extremely rare globally. Their preservation is probably related to high-temperature crystallization followed by rapid cooling. These compositions occur at two of the four investigated volcanic centres (Búðahraun and Berserkjahraun) and indicate a strong influence of crustal magmatic processes on crystal composition and fO_2, which is absent in the other two

locations (Ólafsvíkurenni and Nykurhraun). Spinel and olivine compositions support the tectonically controlled decompression melting of a fertile peridotitic source at elevated mantle temperatures relative to MORB and more reducing conditions than other off-rift magmatism in Iceland.

Key words: spinel; olivine; oxygen fugacity; geothermometry; magma processing; mantle source

INTRODUCTION

Basalts are the product of mantle (peridotite ± pyroxenite) melting and occupy a spectrum of chemical and isotopic compositions reflecting their sources and the magmatic processes that affected them on their way to the surface. A way of examining basaltic magma sources and processing is through olivine and spinel chemistry. Olivine [(Mg, Fe^{2+})$_2SiO_4$] tends to be the first phases to crystallize from a mantle-derived melt and has forsterite contents (Fo = Mg/(Mg + Fe^{2+}) in mol %) that gradually decrease in evolving basaltic melt systems due to the more compatible nature of Mg compared to Fe^{2+}. Additionally, specific trace and minor elements in olivine can be distinctive for the mineral assemblage in the melt source (peridotite versus pyroxenite components) as well as changing chemical conditions over a wide range of magma fractionation (e.g. Sobolev *et al.*, 2007; Howarth & Harris 2017; Nikkola *et al.*, 2019a; 2019b; Rasmussen *et al.*, 2020). Spinel [(Mg, Fe^{2+})(Al, Cr, Fe^{3+})$_2O_4$] is an early forming oxide in basaltic magmas (e.g. Irvine 1965; 1967; Roeder 1994; Kamenetsky *et al.*, 2001; Barnes & Roeder 2001) that is often included in co-precipitating olivine. The combination of olivine and spinel chemistry reflects the physiochemical properties of the magma at the time of their crystallization and can be used as a recorder of temperature (e.g. Ballhaus *et al.*, 1991; Wang *et al.*, 2008; Coogan *et al.*, 2014; Spice *et al.*, 2016; Matthews *et al.*, 2016; 2020), major element chemistry of the changing host magma (e.g. Thy, 1983; Kamenetsky *et al.*, 2001) and, importantly, oxygen fugacity (e.g. Ballhaus *et al.*, 1991; Nikolaev *et al.*, 2016).

Oxygen fugacity (fO_2) can be distinctive for magma source lithology (e.g. Kress & Carmichael, 1991; Novella *et al.*, 2020), magma chamber processes and influences the eruptive potential and style of volcanism (Kolzenburg *et al.*, 2018). Furthermore, the valency of redox-sensitive elements such as Fe, Cr, V, Eu and Ce (e.g. Roeder & Reynolds, 1991; Mallmann & O'Neill 2009; Burnham *et al.*, 2020) can be affected by fO_2 near the quartz-fayalite-magnetite (QFM) buffer (Kress and Carmichael 1991), which is common for terrestrial magmas. Therefore, fluctuations in oxygen fugacity influence the stability and composition of silicate (e.g. Toplis & Caroll, 1995) and oxide species in mafic magmas (e.g. Hill & Roeder 1974; Roeder & Reynolds 1991, Feig *et al.*, 2010). fO_2 near QFM also controls Fe partitioning during melt evolution because Fe^{2+} is less incompatible than Fe^{3+} in mafic systems (Canil *et al.*, 1994; Blundy *et al.*, 2020) and alters the compatibility of redox-sensitive elements in accessory minerals (e.g. Burnham & Berry 2012; van der Meer *et al.*, 2019; Burnham *et al.*, 2020). Additionally, temperature, fO_2 and fluctuations in oxidation state influence the diffusivity of redox-sensitive elements in minerals and are required as input for geospeedometry (e.g. Petry *et al.*, 2004; Dohmen & Chakraborty, 2007; Jollands *et al.*, 2016) and geothermobarometry calculations (e.g. Putirka 2008).

Oxygen fugacity can be constrained through different independent methods. The Fe^{3+} content of primitive basaltic glasses from Iceland has previously been determined via Mössbauer spectroscopy, revealing fO_2 conditions around QFM (Óskarsson *et al.*, 1994) for primitive rift zone lavas, but more reduced conditions of Δlog fO_2 (QFM) −2.5 to −3.1 (at 1240°C) for eruption products from Kistufell, a monogenetic table mountain located in the neovolcanic rift zone close to the inferred centre of the Icelandic plume (Breddam 2002). More recent studies applied micro-XANES spectroscopy to glasses and melt inclusions from Iceland and the Reykjanes Ridge. For instance, Novella *et al.* (2020) combined groundmass glass XANES data from Shorttle *et al.* (2015) with V isotopes and V/Sc to evaluate the fO_2 of Reykjanes ridge magmas and qualitatively state that Fe^{3+}/Fe_{tot} remains stable while the mantle potential temperature, pyroxenite component contribution and source fO_2 increase from the Reykjanes ridge towards Iceland. Hartley *et al.* (2017) examined the Fe^{3+} content in melt inclusions from Laki in South Iceland and concluded that they are slightly oxidized (Δlog fO_2 (QFM) +0.4). Schipper & Moussallam (2017) found varied oxygen fugacities for glassy tephra from Surtsey (Δlog fO_2 (QFM) −0.4 to +0.4) and related the more oxidized conditions to more fertile melt components. Likewise, Nikkola *et al.* (2019a), applied olivine–spinel equilibrium oxybarometry to lavas from Eyjafjallajökull (South Iceland Volcanic Zone) and found Δlog fO_2 (QFM) −0.4 ± 1.0. These results suggest that off-rift volcanism in South Iceland is slightly more oxidized than typical mid-ocean ridge basalt, which has an estimated average Δlog fO_2 (QFM) of −0.2 or +0.1 (Zhang *et al.*, 2018; Berry *et al.*, 2018).

Olivine–spinel equilibrium as an oxybarometer

The use of olivine–spinel equilibrium has some advantages over spectroscopic techniques on volcanic glass and melt inclusions: (1) olivine and spinel are the earliest forming phenocryst phases in basaltic magmas and their chemistry provides information on the composition, temperature and fO_2 of primitive magmas

throughout extensive fractionation in the magma plumbing system; (2) the analysis of minerals allows for the identification of alteration and avoids secondary oxidation in melts during magma degassing (Helgason *et al.*, 1992; Roeder *et al.*, 2003) or through post-entrapment valence changes of sulphur in glasses (Brounce *et al.*, 2017; Nash *et al.*, 2019); (3) it circumvents dependence on spectrum interpretation and standardization (e.g. the re-interpretation of the data of Shorttle *et al.* (2015) by Novella *et al.* (2020) or ongoing debate on the fO_2 of MORB glasses, e.g. by Berry *et al.* (2018) and Zhang *et al.* (2018)); (4) electron microprobe methods are robust, can be applied to glass and minerals alike, are quick, inexpensive and easily replicated; (5) *in situ* analysis supplemented with back-scatter electron images allows results to be integrated with the interpretation of chemical structure (zoning) of the crystals and (6) it allows the direct application of several independent geothermometers.

There are also some limitations to the method: (1) the calculated temperatures and oxygen fugacities remain dependent on empirical laboratory models; (2) the available temperature and fO_2 equations are only calibrated for a certain range of mineral chemistries; (3) calculated fO_2 is only accurate if the minerals are in equilibrium and the temperature is well constrained and (4) the calculation of fO_2 is not very precise ($\pm$0.5 log units), owing to the reproducibility of the calibration data set (Nikolaev *et al.*, 2016). However, the unique strength lies in linking mineral texture with composition, fO_2 and temperature.

We use a selection of olivine–spinel pairs from three transitional to alkaline lavas (Holocene Nykurhraun and Búðahraun and Eemian Ólafsvíkurenni; Kokfelt *et al.*, 2006; Debaille *et al.*, 2009; Rasmussen *et al.*, 2020, Kahl *et al.*, submitted) and a Holocene tephra sample (Kothraunskúla crater, Berserkjahraun; Kahl *et al.*, submitted) from the Snæfellsnes peninsula in western Iceland. Information on the bulk rock compositions of glasses, melt inclusions and groundmass glasses from these and other extrusives from Snæfellsnes is presented in the Supplementary Text; supplementary data are available for downloading at http://www.petrology.oxfordjournals.org and in Kahl *et al.* (submitted). The aim of our study is twofold; (1) to assess the viability of compositionally diverse crystals to record fO_2 during magma fractionation and the effects of potential disequilibrium between spinel and olivine and (2) characterize the temperature, fO_2 and magma fractionation of off-rift magmatism on the Snæfellsnes peninsula, Iceland.

GEOLOGICAL SETTING

The Snæfellsnes Volcanic Zone (SNVZ) is a flank zone represented by Pleistocene–Holocene transitional to alkaline reactivated volcanism superimposed on a zone of weakness formed by the Snæfellsnes–Skagi palaeo-rift that was active between 15 and 7–5.5 Ma (Sigurdsson 1970; Jakobsson 1972; Sæmundsson, 1979; Jóhannesson, 1980; Harðarson 1993; Hardarson *et al.*, 1997; Martin *et al.*, 2011). Volcanism differs from that of the rift zones in Iceland, which invariably produce tholeiite. The oldest volcanic units on the Snæfellsnes peninsula are Tertiary tholeiites erupted along the palaeo-rift, which are overlain by 3.3–0.8 Ma Plio-Pleistocene and $<$0.8 Ma Late Pleistocene–Holocene formations (Harðarson 1993; Thordarson & Larsen, 2007). The Quaternary off-rift volcanic systems of the SNVZ are subdivided from west to east into the Snæfellsjökull, Lýsuskarð and Ljósufjöll volcanic systems (Fig. 1). The crust underlying Snæfellsnes is relatively thin, similar to most of that surrounding active rift zones (Kumar *et al.*, 2007; Rychert *et al.*, 2018). The lithospheric mantle thickens away from the active rift zones (Bjarnason & Schmeling 2009), which consequentially limits and isolates magmatic productivity in the off-rift SNVZ (Kokfelt *et al.*, 2006; Thordarson & Höskuldsson 2008; Peate *et al.*, 2010; Burney *et al.*, 2020; Kahl *et al.*, submitted). Volcanism on Snæfellsnes is not related to the separation of two plates, but Snæfellsnes is situated along the western extension of the dextral transform fault along the MIB (Fig. 1), which traverses central Iceland linking the western and eastern volcanic zones. If the Northern Volcanic Zone extension rate is different from the sum of the extension rate in the western and eastern volcanic zones (inset Fig. 1) then the fracture network in Snæfellsnes probably accommodates this by deformation (Sigurdsson 1970). Quaternary volcanism on Snæfellsnes may therefore be best explained as the result of destabilization of the lithosphere controlled by tectonism (Sigurdsson 1970). Linear chains of volcanic centres along fractures continue offshore in seamounts indicating the slow but continued development of Snæfellsnes as a tectonic and volcanic region (Sigurdsson 1970).

METHODS

Samples were selected from existing thin sections (R04, K1 and K2) and polished one-inch epoxy mounts of olivine separates from crushed basalt from Nykurhraun (M16/SNS 206) and Ólafsvíkurenni (M17/SNS214). The polished and carbon coated samples were analysed using a JEOL JXA-8230 SuperProbe electron microprobe (EMP) housed at the Institute of Earth Sciences, University of Iceland. Olivine grains with spinel inclusions were imaged twice with back-scatter electron mapping (Fig. 2), the first image with brightness and contrast settings set to reveal chemical structure in olivine (spinel appears as saturated white) and a second image with settings optimized for chemical structure in the spinel inclusions (olivines appear black). These images were used to target spot analyses at expected equilibrium and disequilibrium relationships and incorporating olivine zonation where relevant. A total of 177 spinels (420 analyses) included in or associated with 31 olivines (658 analyses) were measured. Spinel

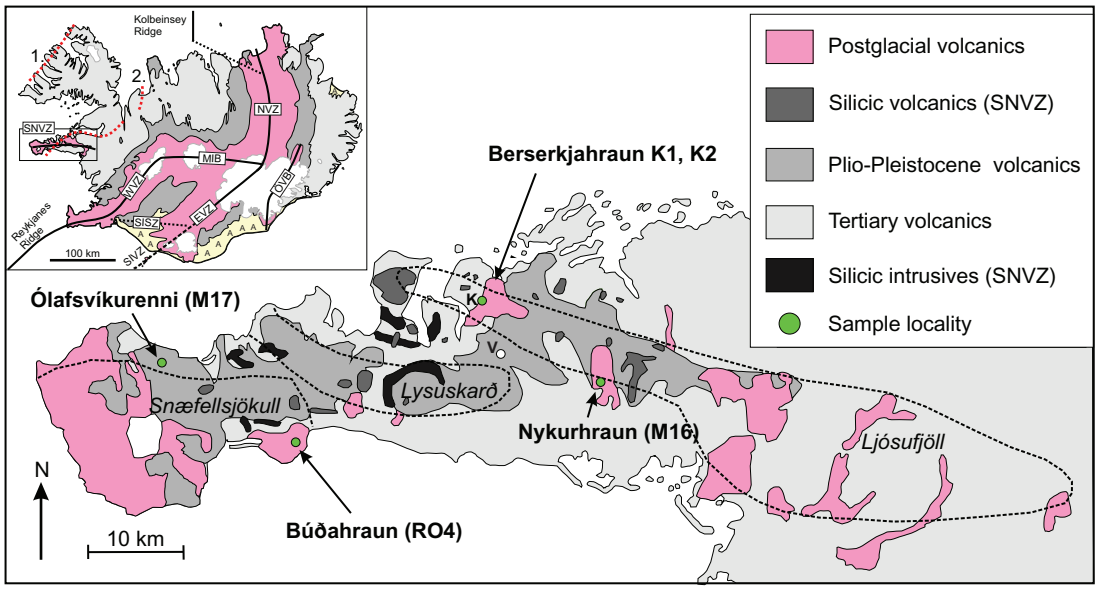

Fig. 1. Geological map of Snæfellsnes after Jóhannesson (1994). Dashed lines indicate the approximate outlines of the three named Holocene volcanic systems. K is the Kothraunskúla crater in the Berserkjahraun lava field. The location of Vatnafell 'V' (Burney *et al.*, 2020) is also indicated. Inset: simplified geological map of Iceland. The main rift segments: Western Volcanic zone (WVZ), Eastern Volcanic Zone (EVZ), Northern Volcanic Zone (NVZ), Mid Iceland Belt (MIB), South Iceland Seismic Zone (SISZ) and the off-rift Öræfi Volcanic Belt (ÖVB), South Iceland Volcanic Zone (SIVZ) and Snæfellsnes Volcanic Zone (SNVZ) are indicated. Red dashed lines indicate Palaeo-rift locations after Jóhannesson (1980) and Harðarson *et al.* (1997), with (1) Northwest Iceland Rift Zone and (2) Snæfellsnes–Skagi Rift Zone.

analyses were combined with multiple nearby olivine analyses to assess chemical equilibrium, yielding 822 unique pairs.

Instrument setup and standards

For the spinel analyses and most of the olivine analyses for M16 and M17, an acceleration voltage of 15 keV and a beam current of 20 nA were used with measurements in spot mode. The routine olivine analyses have an uncertainty that introduces scatter in the trace oxide Al_2O_3. Therefore, high-precision olivine measurements on three spots near each spinel for M16 and M17 and all analyses for the remaining samples were analysed with an acceleration voltage of 15 keV, beam current of 50 nA, a 5 μm spot size and longer counting times (90 s on peak and background) for Al, Ti, Cr and Ni. Olivine spot locations were chosen close to analysed spinel spots. In addition, several profiles through olivines were measured. In olivine, oxides of Si (relative standard error 0.15%), Ti (inaccurate), Al (7%), Fe (0.3%), Mn (4%), Mg (0.15%), Ca (2.5%), Cr (inaccurate) and Ni (2%) were analysed and Smithsonian standards Springwater Meteorite olivine (USNM 2566) and San Carlos olivine (NMNH 111312–44; Jarosewich, 2002) were used as secondary standards (see Supplementary Table). Total oxides for olivine range between 99.1 and 101.2 wt %. For spinel, a collection of certified natural and synthetic standards were used for calibration. Si (inaccurate), Ti (0.5–3.8%), Al (0.35%), Mn (8%), Mg (0.5%), Fe (0.4%), V (10%), Cr (0.37) and Ni (10%) were measured. Spinel Fe^{3+} and Fe^{2+} contents were calculated by stoichiometry and total oxides were calculated accordingly. Analyses with recalculated totals outside 98–101% were discarded. Spinel analyses were further screened to exclude any with SiO_2 above 0.5 wt %, indicating substantial incorporation of silicate in the probed volume (analysed spinel average ~0.1 wt % SiO_2).

Oxybarometry and thermometry

Oxygen fugacities were calculated based on olivine–spinel equilibrium using the formulations of Ballhaus *et al.* (1991) and Nikolaev *et al.* (2016), which have experimental reproducibilities of $\Delta\log fO_2 \pm 0.4$ and ± 0.5, respectively. Crystallization temperatures were assigned on the basis of Al equilibrium between olivine and spinel, T_{AL} (reproducible to $\pm 20^{\circ}C$; Wang *et al.*, 2008; Coogan *et al.*, 2014), except where the amount of Fe^{3+} cations per four oxygen anions in spinel greatly exceeds that of their calibration sample set (calibrated to 0.11 Fe^{3+} per four oxygen, we allow up to 0.22). Olivine–spinel pairs outside this range receive their temperatures from olivine-liquid thermometry ($T_{ol\text{-}liq.}$), calculated according to equation 22 in Putirka (2008) (reproducible to $\pm 44^{\circ}C$) assuming Mg-Fe^{2+} equilibrium ($K_D{}^{ol\text{-}liq}{}_{Mg\text{-}Fe} = 0.30$ Roeder and Emslie, 1970), 1% H_2O content of the melt, and Fe^{3+}/Fe_{tot} appropriate for our fO_2 results. Olivine compositions were paired with published bulk rock compositions (Harðardóttir, 2020) and glass compositions from Snæfellsnes (Kahl *et al.*, submitted). See Supplementary Text for details.

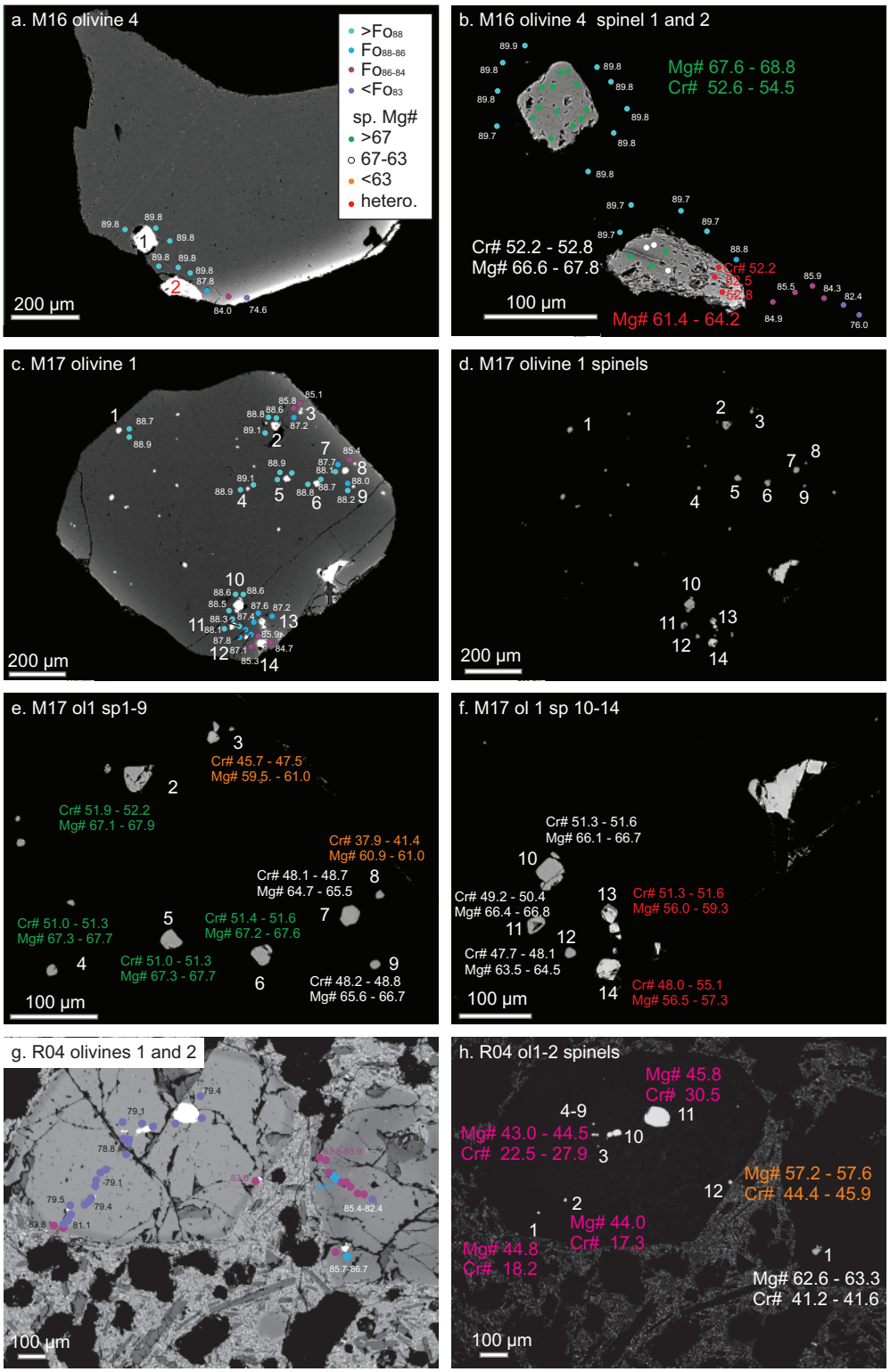

Fig. 2. Back-scatter electron images of representative olivine–spinel pairs. Spot sizes are exaggerated. Spots with high-current olivine analyses and locations for spinel analyses are indicated for M16 olivine 4 in (a). Olivine analyses are colour coded for Fo content in (a), (b) and (c). Spinel compositions are summarized in (b), (e) and (f) with green lettering indicating spinel with Mg# >67, white lettering spinel with Mg# 67–63, orange lettering for spinel with Mg# <63 and red lettering for heterogeneous recrystallized spinel. Spinels 3 and 8 in M17 olivine 1 seem to be in equilibrium with lower Fo olivine, while spinels 13 and 14 in similar Fo olivine have altered compositions and were probably in contact with the surrounding melt through cracks. See "Examples of olivine-spinel disequilibrium" for equilibrium conditions in M16 olivine 4. Representative Fo contents for partial traverses through RO4 olivines 1 and 2 are shown in (g). The spinels and some of their compositional characteristics are given in (h). The spinels in the core of RO4 olivine 1 are Fe-spinel and the spinel in the mantles and rim of RO4 olivine 1 Cr-spinel. The Mg# of the Fe-spinel are very constant but the Cr# increase towards the core with the highest for spinel 11.

(continued)

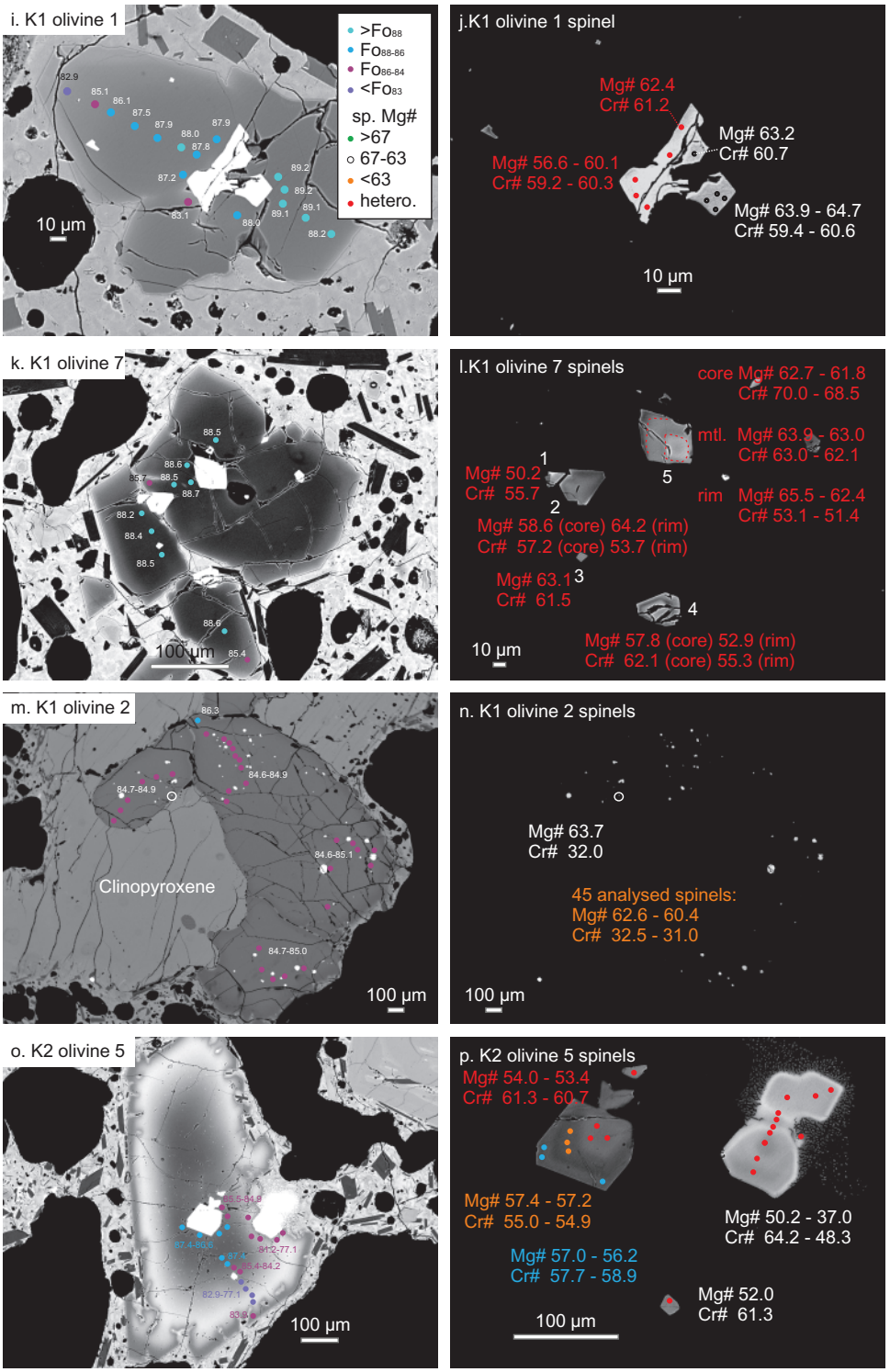

Fig. 2. Continued

Normal zoned K1 olivine 1 (i) contains a cracked heterogeneous spinel grain. The segment to the right in (j) is homogeneous. See "Examples of olivine-spinel disequilibrium" for a detailed description. Normal zoned K1 olivine 7 in (k) and (l) contains spinel grains in contact with cracks or matrix glass. As a result, the spinels are all visibly chemically diverse in (l). The large heterogeneous spinel 5 has relatively uniform Mg# but differences in Cr# increasing from the core towards the rim of the spinel (values in figure). The compositions of the olivine and the spinel are homogeneous except one spinel in a slightly reverse zoned part of the olivine in contact with clinopyroxene. K1 olivine 2 (m) is an olivine macrocryst intergrown with clinopyroxene and contains abundant homogeneous spinel inclusions (n). Complex zoned K2 olivine 5 in (o) contains two large and two smaller spinels. The larger spinels are visibly heterogeneous in p with one spinel recrystallizing within the matrix (also see Fig. 9). The small spinel in the matrix is poorer in Cr than the larger spinel, similar textures were interpreted by Roeder *et al.* (2001) to be associated with rapid cooling. See "Examples of olivine-spinel disequilibrium" for a detailed description.

RESULTS AND DATA ASSESSMENT

Ólafsvíkurenni (M17) and Nykurhraun (M16)

The spinel inclusions from Ólafsvíkurenni (M17) and Nykurhraun (M16) are 50 μm and smaller and occur in several spatial settings in ~1 mm normal zoned olivine (Fig. 2): touching glass, associated with cracks, near melt inclusions, in strongly zoned olivine, in slightly zoned/unzoned olivine. We divide them into homogenous spinel that appears to be in equilibrium and spinel that is heterogeneous in composition and unlikely to be in equilibrium (Fig. 2). Severe spinel disequilibrium is visible in back-scatter electron images through strong density contrast within individual spinel grains (Fig. 2b, j, l and p). More subtle disturbance of spinel is most readily recorded by a shift in Mg and Fe (Fig. 2b; j; also see Scowen *et al.*, 1991). We find that the disequilibrium spinels have heterogeneity exceeding 2% in Mg# (100 Mg/(Mg + Fe^{2+}) in atomic proportions) and/or Cr# (100Cr/(Cr + Al) in atomic proportions) and generally have higher Fe^{3+} at the expense of Al and lower Mg# (Fig. 4). The disequilibrium spinels are featured throughout the figures as red crosses. Spinel completely enclosed by unzoned or slightly zoned olivine is usually homogenous and appears to be in equilibrium. Normal zonation in olivine is uneven around the edges of the crystals suggesting that original grains were broken up (potentially during preparation of the mineral mount).

All equilibrium spinels in M16 are Al-chromites (the atomic proportion of Cr exceeds that of Al, both exceed Fe^{3+}), while M17 contains a continuous range between Al-chromite and Cr-spinel (Al exceeds Cr, both exceed Fe^{3+}; Fig. 4). Spinel in M16 has constant and low TiO_2 (0.48–0.58 wt %) compared to the range of concentrations in spinels from M17 (0.58–1.46 wt %). Similarly, the %Fe^{3+} (100*Fe^{3+}/(Fe^{3+} + Al + Cr)) is lower in M16 (4–8%) than in M17 spinel (5–13%), in accordance with the overall Fe^{3+}/Fe_{tot} in spinel that is limited to 0.20–0.31 for M16 and between 0.23 and 0.37 for M17 (Fig. 5e and f). The Mg# range for equilibrium spinel in M16 is narrow and on the high end (67.4–69.4) compared to that of spinels in M17 (59.7–69.7). Cr# in M16 (48.6–51.7) is likewise high and has a narrower distribution than in M17 (Cr # 33.2–51.5).

The olivine Ni content is lower in M16 than in M17 at comparable Fo (Fig. 3). Olivines in equilibrium with spinel in M16 range to higher $Fo_{88.8–89.9}$ compared to the maximum $Fo_{84.7–89.4}$ for M17 and have higher Ca content with 2142–2431 ppm for M16 and 1795–2224 ppm for M17. Olivine analyses in equilibrium with spinel have Ni* [Ni/(Mg/Fe)/1000] of 0.56–0.61 for M16 and 0.66–0.80 for M17. The samples overlap in 100 Mn/Fe (with M17 1.25–1.74 and M16 1.53–1.61), Ca/Al (with M17 5.2–8.4 and M16 6.5–7.6) and Mn (with M17 1016–1625 ppm and M16 1192–1282 ppm).

The properties of olivine–spinel pairs for these two samples can be grouped based on spinel Mg# (Fig. 6b); primitive spinels have Mg# >67 and are enclosed by unzoned homogeneous olivine with a narrow range of $Fo_{88.5–89}$. Equilibrium olivine–spinel pairs in M16 exclusively have spinel with Mg# >67. The more evolved spinels in M16 are heterogeneous (see Fig. 2a and b). Intermediate equilibrium spinel in M17 has Mg# 63–67 and occurs in olivine with variable $Fo_{86.6–89.3}$. This population of spinel shows a general positive correlation of Mg# with olivine Fo content but is uncorrelated with Cr# in spinel. Lastly, M17 has a substantial population of more evolved spinels with Mg# <63. These occur exclusively in olivine edges with diffuse zoning. Spinels 3 and 8 in olivine 1 (Fig. 2e) are the only low Mg# spinel that appear to be in equilibrium with their surrounding olivine.

Búðahraun and Berserkjahraun

Olivines and spinels from Búðahraun and Berserkjahraun have varied and often complex chemical structure and normal zoned olivines are smaller than those in M16 and M17 (Fig. 2). Kahl *et al.* (submitted) identified several different olivine zoning patterns that can be summarized as different normal zoned olivines with varying core Fo content and complex zoned types with reverse zoned mantles that are again normal zoned with different core, mantle and rim Fo compositions. Spinel occurs in evolved cores, primitive cores, primitive mantles and some normal zoned rims. We observed no spinels in equilibrium with the outermost normal zoned olivine rims between reverse zoned mantles and the carrier melt. In addition, we analysed one olivine macrocryst with abundant spinel inclusions that occurs intergrown with clinopyroxene (Fig. 2m).

R04 (Búðahraun)

The four analysed olivines (1, 2, 4 and 5) in thin section R04 from Búðahraun are each reverse zoned and olivine 2 has complex normal, then reverse zonation surrounded by a normal zoned outer rim (Fig. 2g). The olivines are 0.5–1 mm in the largest dimension and range to more evolved compositions than the normal zoned olivines of M16 and M17. Olivines have $Fo_{75.7–86.8}$ and spinel inclusions occur over the entire range of olivine compositions. Compared to M17, Ni content and Ni* for these mantles is somewhat lower, Ca and Ca/Al are higher at their respective Fo while Mn and 100 Mn/Fe overlap (Fig. 3). Evolved cores with $Fo_{79.6–75.7}$ have lower Ni and Ca and higher Mn contents but similar Ni*, 100 Mn/Fe and Ca/Al compared to the olivine forming the more primitive $Fo_{86.8–83.8}$ mantles (Fig. 3).

Reversezoned olivine mantles (Fig. 2g and h) of olivine 1 ($Fo_{83.8}$) and olivines 2 and 4 ($Fo_{85.7–86.8}$) contain Cr-spinels with uncorrelated Cr# 45.9–41.1 and Mg# 63.3–57.2 (Fig. 5d). TiO_2 (1.2–1.1 wt %), %Fe^{3+} (10.8–9.1) and Fe^{3+}/Fe_{tot} (0.34–0.32) show limited variability, overlap with the highest values for M17 (Fig. 5) and neither correlate with Mg# nor with Cr#. The reverse zoned $Fo_{78.8–79.6}$ cores of olivine 1 contains nine analysed Fe-spinels (Fig. 4) with Mg# 43.2–45.9 and Cr# 17.3–30.5. The

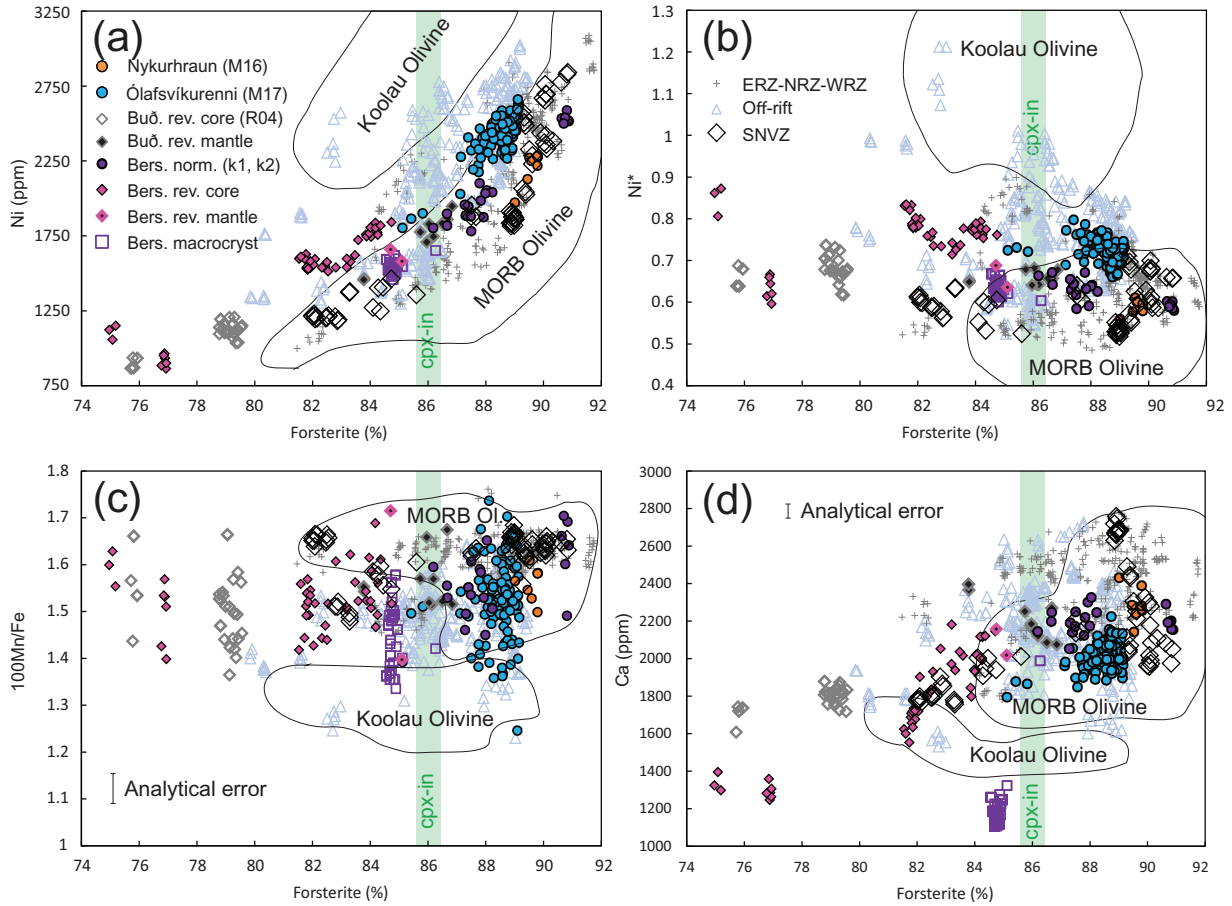

Fig. 3. Chemistry of selected olivines in equilibrium with spinel compared to a compilation of olivine core compositions representative for Iceland (Rasmussen *et al.*, 2020). Data from Rasmussen *et al.* is separated into (1) the Icelandic rift (ERZ-NRZ-WRZ), (2) off-rift including ÖVZ, SIVZ, Hreppar formation and Tertiary basalts and (3) previously published data for SNVZ. Representative fields for MORB and Hawaii (Koolau) from Sobolev *et al.* (2007). Ni, Ni* [Ni/(Mg/Fe)/1000] and 100*Mn/Fe indicate most olivines are MORB-like, suggesting a peridotite dominated source as opposed to a pyroxenitic one. The same can be observed for Ca for the most part, with the exception that Berserkjahraun macrocrystic olivine has low Ca, probably due to the observed co-crystallisation of clinopyroxene. The 'cpx-in' field broadly indicates the Fo content of olivine in equilibrium with the most primitive clinopyroxene from Berserkjahraun and Búðahraun (Mg# 88) using a $K_D^{Mg\text{-}Fe}$ of 1.2 based on >1150°C experiments with olivine in equilibrium with the melt in Loucks (1996). Symbol size exceeds the analytical error for major elements except where indicated.

chemical heterogeneity in spinel is between grains and they individually appear homogeneous. The low $Fo_{75.7–75.9}$ core of olivine 5 hosts five analysed Al-magnetite grains with Mg# 30.2–32.0 and Cr# 11.2–13.0. Spinel TiO_2 contents are high (Fe-spinel: 3.3–6.6 wt % and Al-magnetite: 8.7–11.1 wt %) along with the $\%Fe^{3+}$ (26.3–33.1 and 50.1–54.8 wt %, respectively) and Fe^{3+}/Fe_{tot} (0.34–0.32), which overlaps for Fe-spinel and Al-chromite.

K1 and K2 (Berserkjahraun)

Normal zoned olivines. Olivine with spinel inclusions from Berserkjahraun is subdivided into three types based on their morphology and zonation type. First, we examined ten normal zoned olivines. Compared to normal zoned olivines in M16 and M17, the olivines are markedly smaller, between 100 and 500 μm in the largest dimension, but with similar spinel size of 50 μm and below. Compositionally, they include the most forsteritic olivines analysed; K1 olivine 6 with up to $Fo_{90.9}$ and K1 olivine 11 with up to $Fo_{90.5}$. The remainder of the normal zoned olivines have distinctly lower $Fo_{82.9–89.5}$, much like the olivines in Ólafsvíkurenni (M17). Spinel is heterogeneous (visible density contrast in BSE imaging) when in contact with the matrix or glass inclusions (Fig. 2k, l). Contact between spinel and melt was probably emphasized by the generally limited size of the olivines that occur in clusters (Fig. 2). Only four olivines with $Fo_{86.2–90.9}$ contain homogeneous spinel. Their Ni* (0.58–0.77) and Ca (2052–2325 ppm) are similar to Nykurhraun (M16) and are different from those for Ólafsvíkurenni (M17), while Ca/Al (6.5–11.8) extends to higher values.

Spinel in or near the $Fo_{87.3–90.9}$ cores of the normal zoned olivines is always Al-chromite, two Cr-spinel in the normal zoned $Fo_{86.2–87.3}$ rims of olivine 8 and 9 do not touch glass and appear to have equilibrated with the surrounding olivines. Spinel TiO_2 (0.63–1.23 wt %) is comparable to the range observed for spinel in M17 but

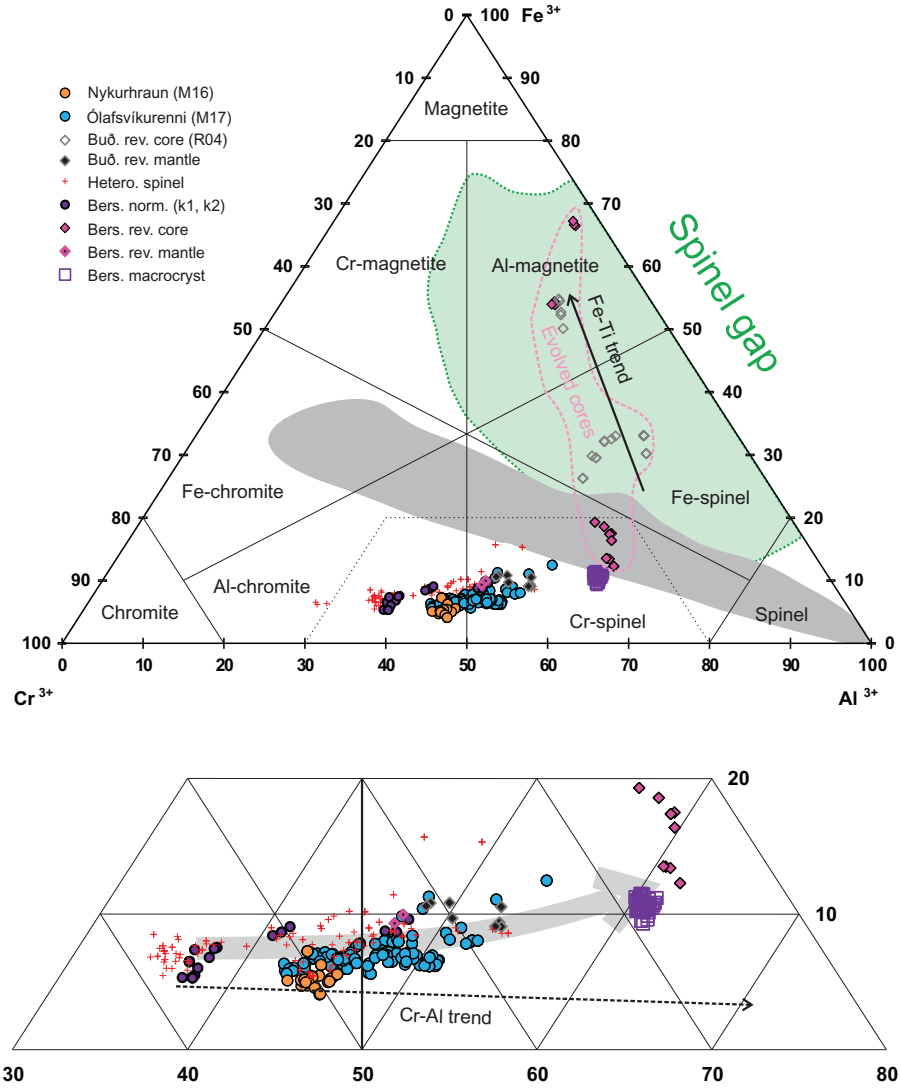

Fig. 4. Classification of spinel based on the atomic proportions of the trivalent ions Fe^{3+}, Cr and Al. Spinel in reverse zoned olivines from RO4 are Fe-spinel or Al-magnetite in cores and Cr-spinel in higher Fo mantles. For K1 and K2 reverse cores have either magnetite (K1 ol3, k1 ol10 and K2 ol6) or Cr-spinel (K2 ol2 and K2 ol4) in the core and Cr-spinel in the mantles (K1 ol4 and ol10). Spinel in the mantles of reverse zoned olivines plots with spinel in normal zoned olivine. The compositions of spinel occurring in evolved cores is encircled by the pink dashed line. Cr-Al and Ti-Fe trends after Barnes & Roeder (2001), the latter traverses the 'spinel gap' and consists of rare Fe-Al-rich spinels (Roeder 1994; Barnes & Roeder, 2001). Shaded field shows the range of spinel compositions used for calibration by Nikolaev *et al.* (2016). The lower panel shows a close-up of the Al-chromite and Cr-spinel samples with a grey arrow indicating the trend of the samples which slightly deviates from the Cr-Al trend that represents the long-term isothermal equilibration between spinel and olivine in cumulates according to Irvine (1967). Symbol size exceeds analytical error.

the Berserkjahraun Al-chromites have a significantly higher Cr# (54.5–60.9) than spinel in M16 and M17. The $\%Fe^{3+}$ (5.3–9.6 wt %), Fe^{3+}/Fe_{tot} (0.25–0.32) and Mg# (60.2–70.0) fall within the range of compositions observed in M17.

Olivine macrocryst. K1 olivine 2 (Fig. 2m, n) is a >1 mm large anhedral olivine that appears to be an aggregate of three large, rounded grains intergrown with clinopyroxene, suggesting it might be part of a small wehrlitic xenolith. The olivine aggregate contains >50 spinel inclusions of up to 40 μm, of which 46 were analysed. The interior of the olivine has a limited compositional range with $Fo_{84.6–85.1}$ (Fig. 3), but a thin reverse rim of $Fo_{86.3}$ (Fig. 2m) containing sparse spinel. Olivine compositions of the reverse zoned rim are similar to the low-Fo contents of normal zoned olivines from Berserkjahraun. The interior of the olivine has similar Ni* (0.60–0.67), 100 Mn/Fe (1.33–1.58), but lower Ca/Al (5.0–8.0) than normal zoned olivine from Berserkjahraun and drastically lower Ca (1107–1323 ppm) than any other Icelandic olivine composition reported by Rasmussen *et al.* (2020) (Fig. 3d) and Nikkola *et al.* (2019a).

Spinels in the core ($Fo_{84.6–85.1}$) have restricted Mg# 60.4–62.6, Cr# 31.0–32.5, TiO_2 1.49–1.72 wt %, 9.3–11.5 $\%Fe^{3+}$ and Fe^{3+}/Fe_{tot} 0.31–0.37. The only notable difference between a spinel in the reverse zoned rim ($Fo_{86.3}$) compared to spinels in the core is the elevated Mg#

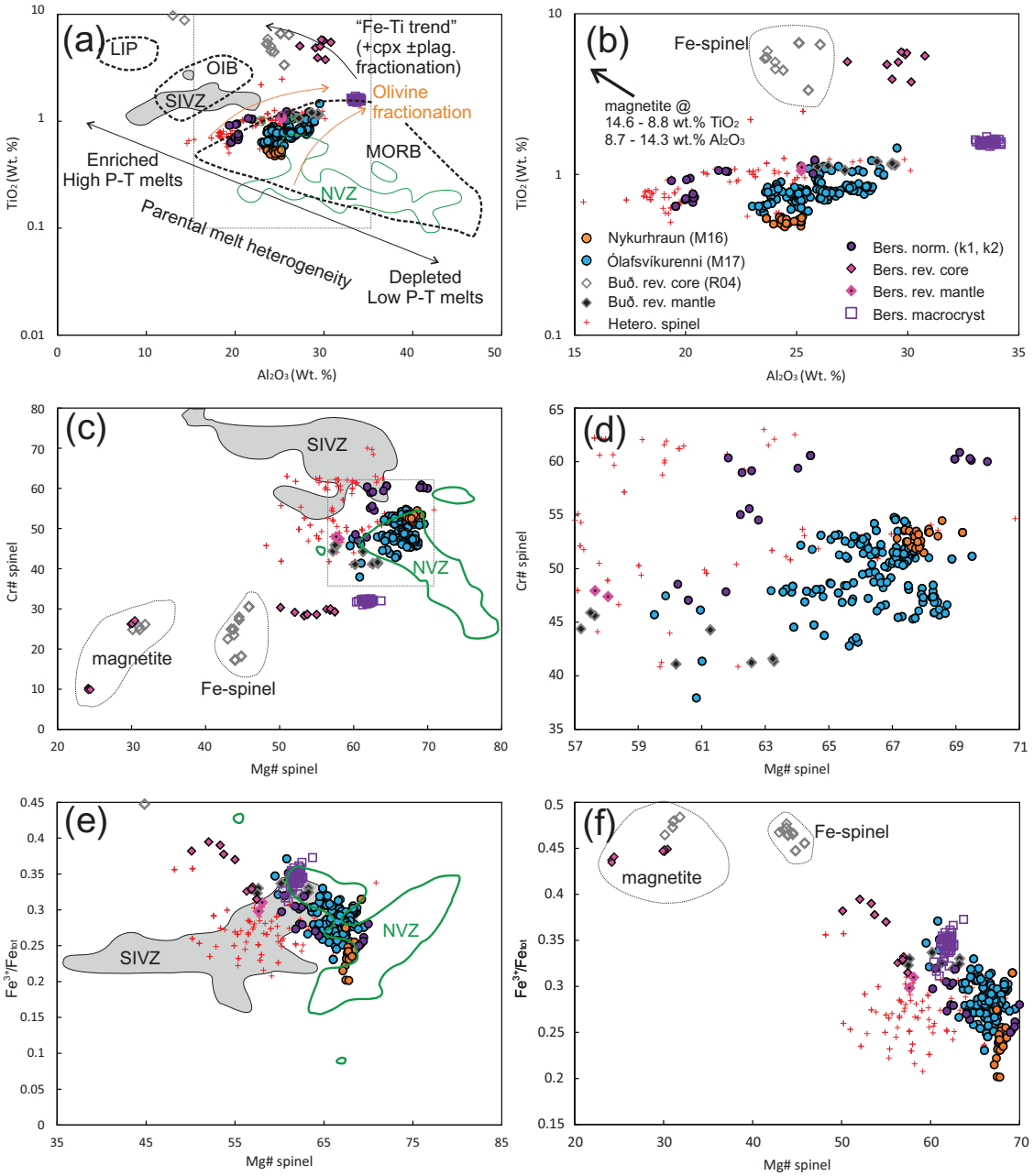

Fig. 5. Chemistry of spinel from Snæfellsnes (this study) compared to spinel from the transitional alkaline basalts of the South Iceland Volcanic Zone (SIVZ) as a grey field (Brattaskjól and Hvammsmúli from Nikkola *et al.*, 2019a) and tholeiites from the Northern Volcanic Zone (NVZ) outlined in green (Matthews *et al.*, 2016). Fields for MORB, OIB and LIP for spinel within >Fo_{84} olivine in (a) are from Kamenetsky *et al.* (2001). The effect of heterogeneous parental melts (Kamenetsky *et al.*, 2001) and trajectories corresponding to olivine fractionation and Ti-Fe trends are also included (Roeder *et al.*, 1994; Barnes & Roeder 2001), cpx: clinopyroxene and plag: plagioclase. Compositions of all spinels from Snæfellsnes in olivines with >Fo_{84} fall in or close to the MORB field in (a). (b), (d) and (f) show the variation within Snæfellsnes with a focus on the more primitive spinel. For one of each pair of panels, the populations of Fe-spinel and Al-magnetite are circled. The remaining compositions are Cr-spinel and Al-chromite.

63.8 and Fe^{3+}/Fe_{tot} 0.37 in the former. The spinel compositions are unique in the sample set, having lower Mg# and Cr# but higher TiO_2, Al_2O_3 and Fe^{3+}/Fe_{tot} compared to spinel in normal zoned olivine (Figs 5, 6).

Reverse zoned olivines. Five reverse zoned olivines from K1 and K2 were analysed. Olivines are 300–600 μm, except K2 ol6, which is >1 mm. All grains have outer rims of Fo_{81-82} surrounding Fo_{84-86} mantles that gradually transition inward to evolved cores, reaching minima of Fo_{75-82}. The mantles of K1 ol4 and K1 ol10 ($Fo_{84.7–85.1}$, Ni* 0.64–0.69) are mostly identical to the macrocryst (K1 ol2) but with higher Ca (2019–2147 ppm) and Ca/Al (9.9–11.7). Evolved olivine core compositions are highly variable due to the diffuse boundaries between mantles and cores. Compositions are $Fo_{75.0–84.7}$ with varying Ni* (0.58–0.87), 100Mn/Fe (1.39–1.69) and

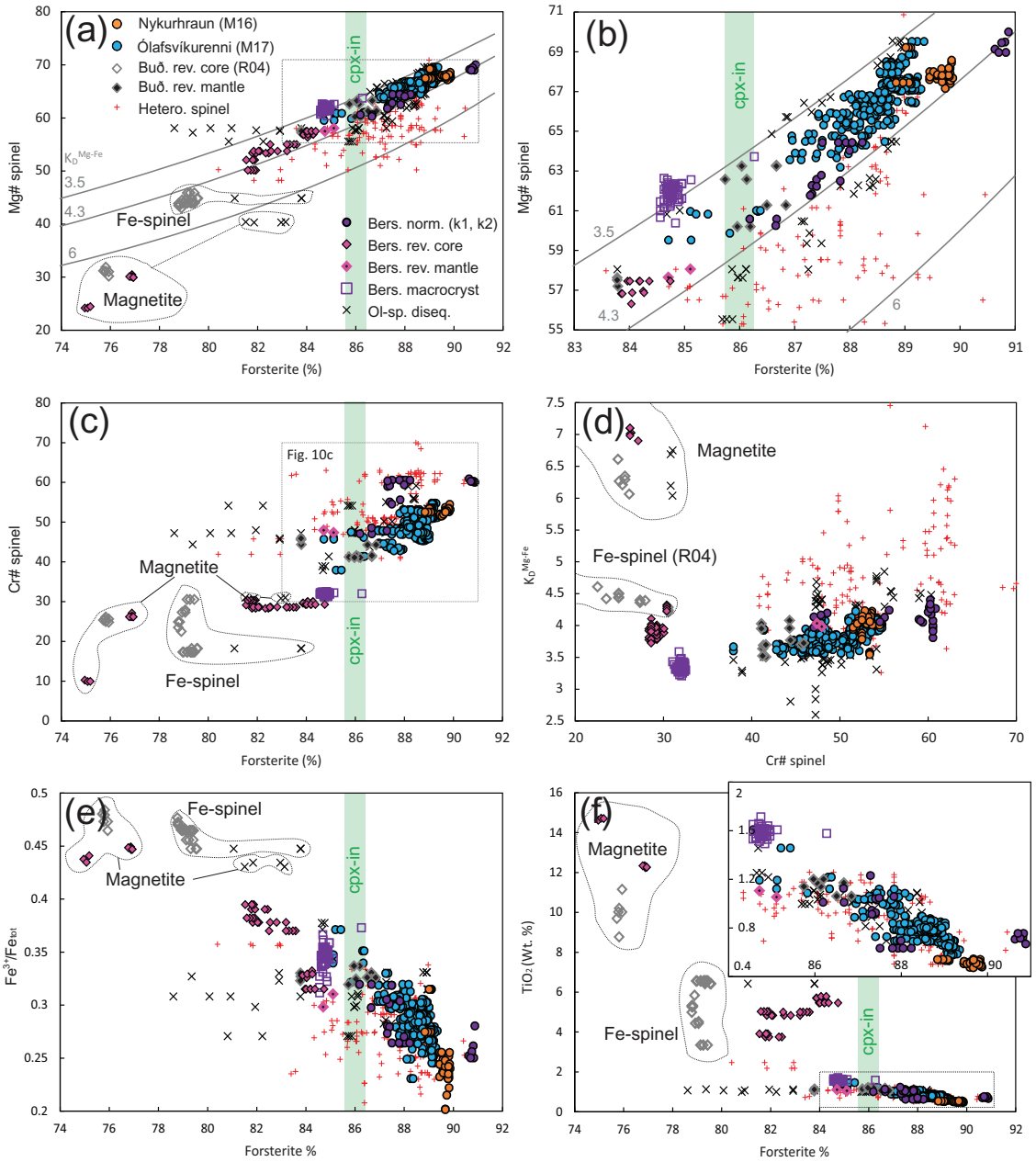

Fig. 6. Combined olivine and spinel data. (a) The relationship between the Mg# in spinel and the Fo content of olivine (or olivine Mg#). Curves are the calculated reference equilibrium lines for different values of the exchange coefficient $K_D^{Mg\text{-}Fe} = (Mg/Fe)_{olivine}/(Mg/Fe^{2+})_{spinel}$, 3.5, 4.3 and 6. (b) Detail of high Mg# spinel. (c) Spinel Cr# as a function of the Fo content of the enclosing olivine. (d) $K_D^{Mg\text{-}Fe}$ and Cr# in spinel for the olivine–spinel pairs correlate positively, except for spinel with Cr# <30, occurring in evolved cores of reverse zoned olivines and coinciding with elevated Fe^{3+} (>12%). (e) The Fe^{3+}/Fe_{tot} for spinel compared to the surrounding equilibrium olivine. (f) TiO_2 content of spinel compared to Forsterite content of the surrounding olivine. Inset shows the relationship for Ti-poor spinel.

Ca/Al (6.9–11.6) but Ca is generally low (1247–2181 ppm).

The mantles of K1 ol4 and K1 ol10 contain Cr-spinels (Cr# 47.4–47.9, TiO_2 1.1 wt %, 9.3–9.9 $\%Fe^{3+}$ and Fe^{3+}/Fe_{tot} of 0.30–0.31) that are identical to some spinels contained in normal zoned olivines from Berserkjahraun, with the exception of having somewhat lower Mg# (57.6 and 58.0). Cr-spinel also occurs in the core regions of K2 ol2 and K2 ol4 $Fo_{81.5–84.7}$. These have a wide range in Mg# (50.1–57.5), 12.3–19.3 $\%Fe^{3+}$ and Fe^{3+}/Fe_{tot} (0.31–0.39) at a narrow range of Cr# (28.3–30.4) and relatively limited but high TiO_2 (3.8–5.8 wt %). K1 ol3 (~Fo_{75}), K1 ol10 (~Fo_{81}) and K2 ol6 (~Fo_{77}) cores contain Al-magnetite (similar to RO4 ol5, $Fo_{75.7–75.9}$), with Cr# 9.9–31, Mg# 24.1–40.4, 12.2–14.7 wt % TiO_2, 42.0–67.2% Fe^{3+} and Fe^{3+}/Fe_{tot} of 0.43–0.45. Al-magnetite contained in K1 ol10 is considered unlikely to be in equilibrium because of the strong Fo gradient within the

core of the grain ('ol-spinel disequilibrium' symbols marked as 'magnetite' in figures).

Examples of olivine–spinel disequilibrium

The chemical profile of olivine and spinel combined with differing diffusion and equilibration speeds for different elements and between the different minerals can make the selection of equilibrium pairs difficult. Therefore, several samples with zoned olivine and spinel were specifically targeted to test the effects disequilibrium can have on calculated fO_2 and temperatures. The pressure was kept at 0.5 GPa and for choice of thermometer and oxybarometer see the discussion in a later section.

M16 olivine 4 (Fig. 2a, b)

M16 olivine 4 is a fractured normal zoned olivine with $Fo_{74.6–89.8}$ containing two large (>50 μm) spinels. Spinel 1 is situated in the unzoned part of the olivine ($Fo_{89.7–89.9}$), is homogeneous with Mg# 67.3–68.5, Cr# of 52.6–54.5 resulting in $K_D^{Mg\text{-}Fe}$ of 4.0–4.2 and yields Δlog fO_2 (QFM) between −0.37 and −0.08. Spinel 2 is situated in the sharp normal zoned part of the olivine and has heterogeneous Mg# 61.4–67.8 but retains homogeneous Cr# 52.1–52.8. The varied spinel and olivine compositions are matched to derive extreme $K_D^{Mg\text{-}Fe}$ ranging between 1.8 and 5.0. Spinel 2 matched with a zoned part of the olivine to arrive at a similar $K_D^{Mg\text{-}Fe}$ of 4.0–4.2 returns a lower Δlog fO_2 (QFM) between −0.53 and −0.39. Severe disturbance of fO_2 is observed when the spinel is paired with directly adjacent normal zoned olivine, reaching values as low as Δlog fO_2 (QFM) of −1.5 for $Fo_{82.3}$ or even −2.3 for $Fo_{74.6}$ (not shown in figure).

K1 olivine 1 (Fig. 2i, j)

K1 olivine 1 is a normal zoned olivine with $Fo_{82.9–89.2}$ containing several spinel grains. Multiple spots on the central large ∼40 μm irregular spinel (fractured into two chemically distinct fragments) were analysed and compared to olivine of differing $Fo_{82.9–89.2}$. One of the segments is heterogeneous (mainly in Mg-Fe) trending towards more evolved compositions (Mg# 56.6–63.2, Cr# 59.2–61.2 and TiO_2 0.69–0.92 wt %; $n = 6$) compared to the second more homogeneous part (Mg# 63.9–64.7, Cr# 59.4–60.6 and TiO_2 0.63–0.70 wt %; $n = 4$). From the texture and chemistry, it is clear that the heterogeneous part (bright in BSE) of the spinel was altered diffusively, probably due to the contact with the melt through cracks traversing the spinel as well as the olivine. When representative portions of both sides of the spinel are paired with olivine of different Fo content, two parallel arrays are formed on a diagram of Fo content against fO_2 (Fig. 7a). The heterogenous spinel yields higher oxygen fugacities than the pristine spinel portion when paired with the same olivine composition. Pairing both parts of the spinel against the entire observed range of olivine compositions results in an array of $Fo_{82.9–89.2}$ and $K_D^{Mg\text{-}Fe}$ between 2.6 and 6.2 (Fig. 7b). An important observation is that pairing the homogeneous high Mg# spinel with the nearby olivine core with composition $>Fo_{88.5}$ yields $K_D^{Mg\text{-}Fe}$ >4.4. Considering the other normal zoned olivines (see later section), these are not in equilibrium. The effect is a projection of overly oxidized compositions of up to Δlog fO_2 (QFM) of 0 compared to −0.37 to −0.23 for the spinel paired with olivine with equilibrium $K_D^{Mg\text{-}Fe}$. Therefore, pairing the most primitive spinel with the most primitive olivine is no guarantee for obtaining the right compositional pair. Additionally, while olivine can be paired to the recrystallized spinel at an apparent equilibrium $K_D^{Mg\text{-}Fe}$, it is doubtful if this will yield reasonable temperatures and oxygen fugacities because the Cr# is still identical to the homogeneous higher Mg# spinel, indicating a decoupling of ions of different charge. The temperatures on the other hand, are not affected by changes in Mg# in spinel and are hardly affected by a change in Cr# in spinel due to recrystallization (Figs 7c and 8d) but are controlled by olivine Al content (Fig. 8c).

K2 olivine 5 (Fig. 2o, p)

K2 ol5 has complex compositional zoning with a normal zoned core ranging from $Fo_{87.4}$ down to $Fo_{75.6}$ with a narrow mantle of $Fo_{83.9}$ and an outer rim with a composition of $Fo_{81.0}$. The core contains three spinels and a fourth large spinel occurs in contact with the matrix where it recrystallized within the melt (Fig 2p). The network of small spinel grains within the melt indicate crystallization up to a point of rapid cooling (Roeder *et al.*, 2001). The spinel in contact with the matrix (Spinel 4 in Fig. 7) has widely varying compositions with Mg# 37.0–50.2, Cr# 48.3–64.2 and TiO_2 between 0.7 and 3.0 wt % (Fig. 9). Combined with surrounding olivine compositions ($Fo_{77.1–81.2}$) the spinel compositions have $K_D^{Mg\text{-}Fe}$ 4.1–6.9, Δlog fO_2 (QFM) between −1.3 and 0.4 and T_{AL} between 1178 and 1264°C. By contrast, the large spinel in the centre has higher Mg# 53.4–57.0, and somewhat less scattered and overlapping Cr# 57.2–61.3 and TiO_2 between 0.77–0.91. Spinel combined with the surrounding olivine core ($Fo_{84.9–87.4}$) has $K_D^{Mg\text{-}Fe}$ 4.8–5.6, Δlog fO_2 (QFM) between −0.54 and −0.10 and T_{AL} between 1210 and 1295°C. Two small spinels appear to be relatively homogeneous (Mg# 58.0 and 52.2 and Cr# 59.0 and 61.3) and are located in the core and on the edge of the core of the olivine. Due to their presence in strongly zoned olivine, it is doubtful if equilibrium with olivine is obtained for any spinels in this olivine.

DISCUSSION

Choice of oxybarometer, thermometer and pressure

The fO_2 of olivine–spinel pairs are calculated based on the oxybarometers published in Ballhaus *et al.* (1991) developed for peridotites (with orthopyroxene present) and Nikolaev *et al.* (2016) calibrated to a wider range of

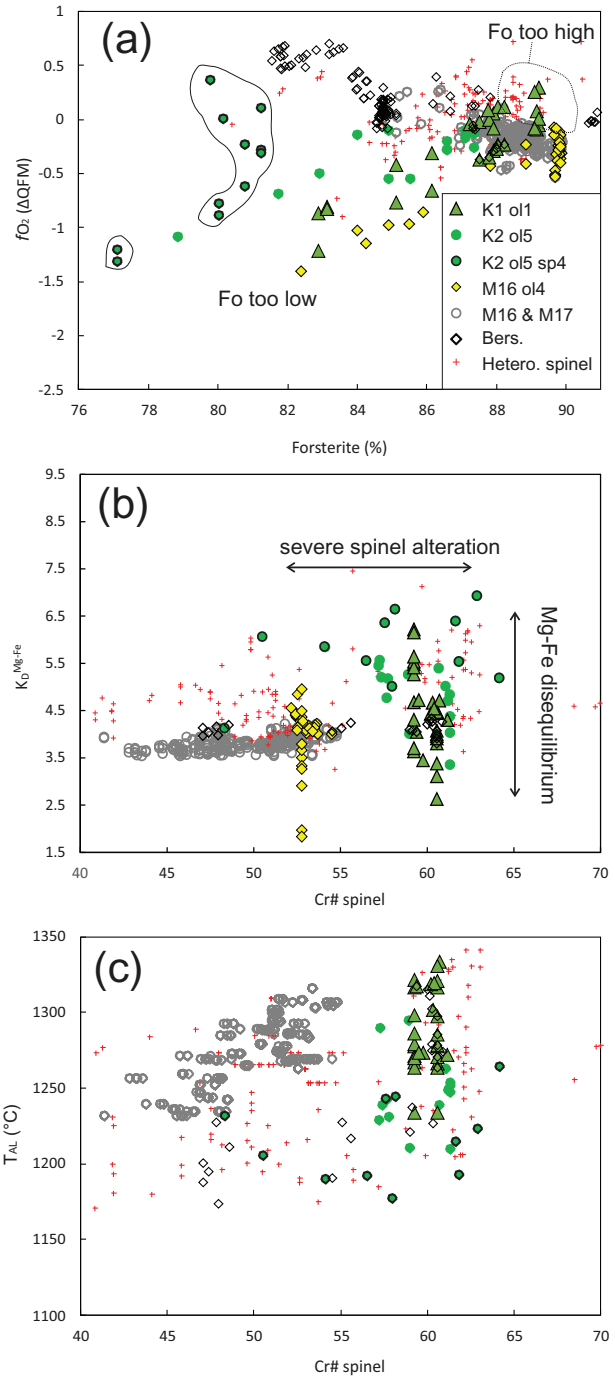

Fig. 7. Effects of disequilibrium pairs and spinel alteration on calculated temperature and fO_2. Analyses for Nykurhraun (M16), Ólafsvíkurenni (M17), Berserkjahraun (K1 and K2) and heterogeneous spinel are included for reference. M16 ol4 is not featured in (c) because high-precision olivine analyses are unavailable for each analytical pair in this sample.

lithologies. Nikolaev *et al.* (2016) reported a systemic offset of the Ballhaus *et al.* (1991) fO_2 calculations of +0.6 to +1.3 log units (at mildly reducing conditions). A similar offset between the two methods is also visible in our data set: the Ballhaus *et al.* (1991) oxybarometer gives fO_2 that are +0.4 to +1.5 log units relative to the Nikolaev *et al.* (2016) method, the discrepancy increases with more evolved spinel and olivine compositions (Fig. 8a). We use the calibration by Nikolaev *et al.* (2016) because of the wider calibration data set, which includes basalts.

Three thermometers: olivine–spinel Al equilibrium (T_{AL}; Coogan *et al.*, 2014), olivine-melt thermometry ($T_{ol\text{-}liq}$; Putirka, 2008) and olivine–spinel Mg-Fe exchange thermometry (T_{Ball91}; Ballhaus *et al.*, 1991, calibrated for peridotites) are considered. T_{AL} and $T_{ol\text{-}liq}$ return generally similar results (Fig 10a), and we use T_{AL} where possible (see the Methods section) because it is resistant to overprinting and ideal for capturing the crystallization temperature. $T_{ol\text{-}liq}$ is used for samples where the Fe^{3+} content in spinel exceeds the calibration dataset for the T_{AL} method. For Al-magnetite, T_{Ball91} greatly over-estimates the temperature and only Fe-spinels give consistent $T_{ol\text{-}liq}$ and T_{Ball91}. T_{Ball91} yields temperatures of 850–1026°C for Al-chromite and Cr-spinel. These temperatures are consistently lower than either $T_{ol\text{-}liq}$ or T_{AL} by at least 150°C and up to 400°C (Fig. 8b). Olivine–spinel pairs from the tephra sample from Berserkjahraun have somewhat higher T_{Ball91} than those for other locations. This is consistent with the diffusion-sensitive T_{Ball91} following the rate of post-emplacement cooling (e.g. Kamenetsky *et al.*, 2001) but does not result in reliable absolute temperature estimates.

Previous clinopyroxene-melt barometry for magmatic systems on Snæfellsnes revealed the predominance of two crystallization levels at different crustal depths. Berserkjahraun and Búðahraun record pressures at ~0.3 and ~0.5 GPa Kahl *et al.* (submitted) and Vatnafell at <0.4 and ~0.6 GPa Burney *et al.* (2020), both in the mid-upper crust and in the lower crust, approaching Moho depth. The olivine macrocryst and reverse zoned olivines have composition up to ~$Fo_{86\text{-}87}$ (Fig. 3), in equilibrium with Mg# up to 88 for clinopyroxene (assuming $K_D^{ol\text{-}cpx}{}_{Mg\text{-}Fe} = 1.2$ at ~1180°C; Loucks, 1996). Therefore, the pressure for these olivine–spinel pairs is set to 0.5 GPa. The presence of Cr-spinel and Al-chromite in high-forsterite (>Fo_{86}) olivine indicate crystallization before the most primitive clinopyroxenes (see Figs 3, 6 and 9). This is further strengthened by the observation that the presence of clinopyroxene would suppress the formation of Cr-rich spinel species through the depletion of the magma Cr budget (e.g. Hill & Roeder 1974; Roeder, 1994; Barnes & Roeder 2001). Therefore, the Cr-spinel, Al-chromite and their primitive olivine hosts formed below the deepest clinopyroxene-bearing parts of the magmatic system. Olivine with >Fo_{90} forms in melts in equilibrium with mantle peridotite (e.g. Albarede, 1992; Putirka *et al.*, 2007), further suggesting a sub-crustal origin. Without a reliable barometer for olivine–spinel pairs, we assume a conservative pressure for these olivines at 0.7 GPa, corresponding to the estimated local Moho depth (~25 km).

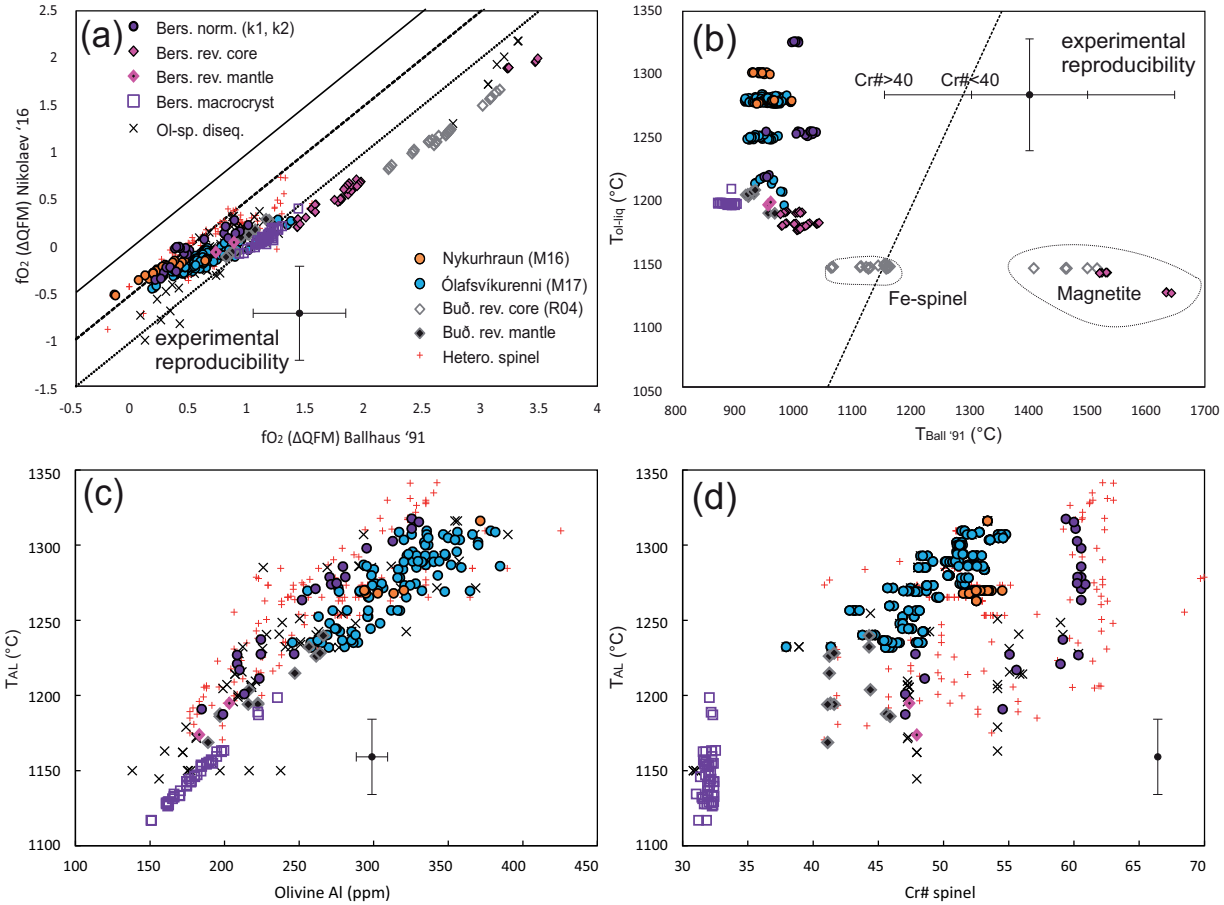

Fig. 8. Comparison of oxybarometers and thermometers. (a) Comparison of fO_2 calculated by the methods of Nikolaev *et al.* (2016) and Ballhaus *et al.* (1991) at identical temperature and pressure. Solid line traces 1:1 with dashed and dotted lines 0.5 and 1 log unit lower, respectively. (b) Comparison of olivine-liquid temperatures (Putirka, 2008) with spinel–olivine Mg–Fe exchange temperatures (Ballhaus *et al.*, 1991). Line traces 1:1. (c and d) Al content in olivine and Cr# in spinel plotted against T_{AL}. Uncertainty on $T_{Ball'91}$ is unspecified but in the order of ±250°C for spinel Cr# < 40 and ±100°C for Cr# < 40, see Fig. 7b in Ballhaus *et al.* (1991).

Assessment of equilibrium assemblages

Natural olivine and spinel experience changing ambient magmatic conditions that can alter their chemical composition after crystallization. To acquire accurate temperature and fO_2 estimates, a careful assessment of the chemical equilibrium between olivine and spinel is essential. Establishing equilibrium pairs starts with mapping both olivine and spinel chemical structures using back-scatter electron images (Fig. 2). From the images, a primary division can be made between (1) spinel that is completely enclosed by homogeneous olivine, (2) spinel that is enclosed by zoned olivine and (3) spinel that has been in contact with the melt on the edge of an olivine or near a crack through the encasing olivine. These three situations correspond to deteriorating conditions for the olivine–spinel equilibrium. Spinel completely enclosed by homogeneous olivine is homogeneous as well. Mg and Fe^{2+} are the only major elements shared by both phases and their relative equilibrium distributions can be easily calculated. The distribution ($K_D^{Mg\text{-}Fe}$) ranges between 2 and 12 for terrestrial mafic and ultramafic rocks (Kamenetsky *et al.*, 2001) and is greatly influenced by Cr# in spinel (Fig. 6d; Sack & Ghiorso, 1991a), Fe^{3+} content of spinel (Sack & Ghiorso, 1991a), temperature and cooling rate (e.g. Irvine , 1967; Scowen *et al.*, 1991). Homogeneous olivine (>Fo_{87}) paired with homogeneous Al-chromite and Cr-spinel (with moderate %Fe^{3+} between 4.1–12.5%) in the basaltic lavas and tephra has a $K_D^{Mg\text{-}Fe}$ between 3.5 and 4.3. This range in $K_D^{Mg\text{-}Fe}$ provides a crude but useful indicator for equilibrium conditions applicable to olivine–spinel pairs from the SNVZ. Differences in cooling rate may in part explain why spinel and normal zoned olivine from the Berserkjahraun tephra samples have $K_D^{Mg\text{-}Fe}$ on the high end of this range (Fig. 6a, b, d). Due to the additional influence of Fe^{3+}, spinel in evolved cores is assessed based on the homogeneity of the spinel and the surrounding olivine rather than the value of $K_D^{Mg\text{-}Fe}$.

Spinel in normal zoned olivine

Aluminium, Cr and sometimes Ti are major elements in spinel but incompatible in olivine. Due to the slow diffusion of Cr and Ti and apparent lack of any diffusion of Al in olivine (Roeder & Campbell, 1985; Spandler &

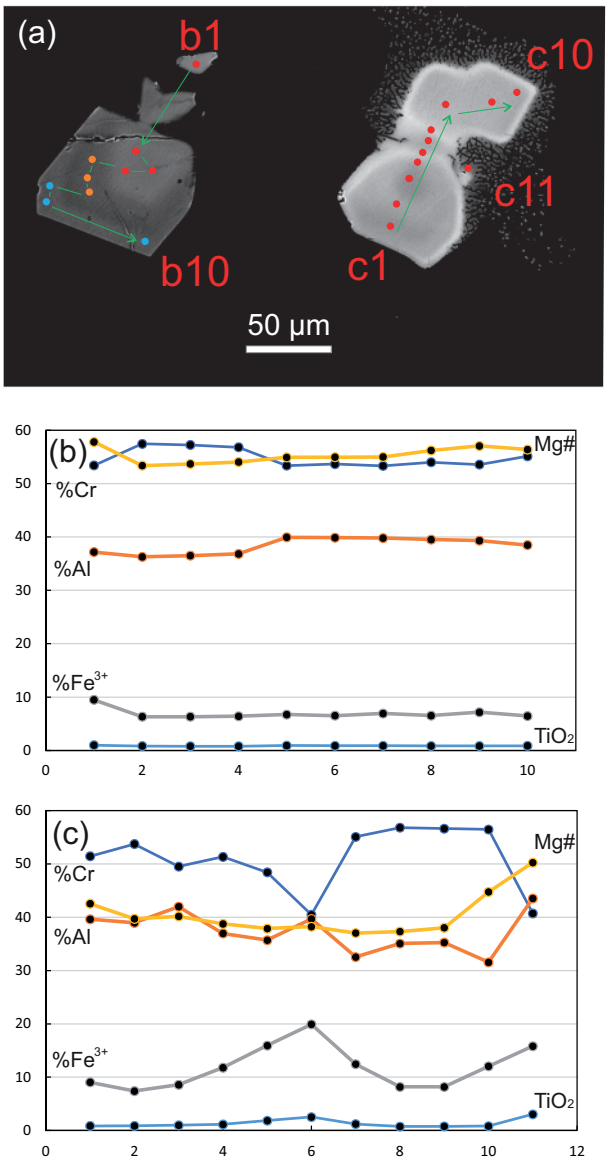

Fig. 9. Profiles through spinel grains in K1 olivine 5. Analytical spots are indicated in (a), transect (b) is through spinel enclosed by zoned olivine, transect (c) is through spinel enclosed by olivine and matrix (Fig. 2o). Trivalent ions as a percentage: %Cr = molar 100Cr/(Cr + Al + Fe^{3+}) etc. TiO_2 in weight percentage.

O'Neill, 2010; Cherniak & Liang, 2014; Coogan *et al.*, 2014; Mutch *et al.*, 2021) these elements are effectively shielded by the surrounding olivine. This is further emphasized in cases where spinel is surrounded by diffusely zoned olivine. Herein, spinel can either be homogeneous in terms of Mg# and adjusted to enclosing zoning in olivine, attesting to the faster Mg-Fe^{2+} diffusion in spinel than in olivine, or be visibly heterogeneous in Mg# (corresponding to >2% difference within a grain). In both cases, the Cr# of spinel can remain unaffected. This implies that the diffusion speed of Mg-Fe^{2+} in spinel is higher than in olivine and both exceed the rate at which Cr# and TiO_2 in enclosed spinel can change (also see: Allan 1994; Roeder *et al.*, 2001; Vogt *et al.*, 2015). Sometimes, the Cr# of entire spinel grains can decrease with Fo content in normal zoned olivine. This is probably related to spinel being captured by growing olivine in evolving melts rather than diffusive lowering of the Fo content of encapsulating olivine. In cases where olivine is zoned but spinel is homogeneous, the fO_2 may be derived after the olivine and spinel compositions have been screened for their appropriate $K_D^{Mg\text{-}Fe}$ (established by spinel of similar composition in unzoned olivine) by analysing olivine with different Fo contents surrounding the spinel. Accurate matching is important because Mg-Fe^{2+} disequilibrium strongly affects the calculated fO_2 (Fig. 7) and can be difficult to identify in BSE imaging. For K1 olivine 1 (Fig. 2k, j), for example, the primitive homogeneous part of the spinel is not in equilibrium with the most primitive nearby olivine and matching these would lead to a systematic fO_2 overestimation of ~0.25 log units. Underestimating the Fo content in olivine can have effects spanning several log units (Figs 7a and 10a, e). The resulting near-linear positive correlations between fO_2 and Fo are extremely suspect (see Fig. 7a, M16 ol4) and show up when olivine and spinel are in various states of Mg-Fe^{2+} disequilibrium. This is an obvious challenge when pairing of equilibrium spinel and olivine in reverse zoned rims with a Fo gradient. The pairs that are included as equilibrium assemblages all have homogenous spinel and fall within the $K_D^{Mg\text{-}Fe}$ window (3.5–4.3) when matched with immediately adjacent olivine compositions. For these spinel–olivine pairs, fO_2 correlates negatively with Mg# in spinel and Fo content in olivine, fortifying the assumption that the spinels are in equilibrium with their surrounding olivine mantles. One olivine containing spinel (K1 ol6) probably suffers from a slight overestimation of the $K_D^{Mg\text{-}Fe}$ even though the spinel is located within a homogeneous core of a normal zoned olivine. Apart from having a fO_2 that falls off a trend with Fo content in olivine (highest Fo data points in Fig. 11a), the spinel has low %Fe^{3+} and Fe^{3+}/Fe_{tot} compared to other samples with the same fO_2 (Supplementary Fig. 1). This sample is nevertheless included because the slight discrepancy does not affect T_{AL} and the composition of the olivine and spinel are useful as an end-member because of its uniquely primitive composition with $Fo_{90.6–90.9}$ and Cr# 56.4–57.6.

Heterogeneous spinel

Spinel in contact with late-stage melt is often spectacularly zoned in Cr# as well as Mg#, which is visible in BSE images (e.g. Fig. 2j, l, p) where transient chemical gradients are captured upon cooling. Heterogeneity is more common for spinel with high Cr#, probably because of the large chemical contrast between the primitive melts from which they crystallized and the more evolved lavas that erupted them. Some of the tendencies for heterogeneous spinel are exemplified by the spinel compositions in K2 ol5, where a heterogeneous

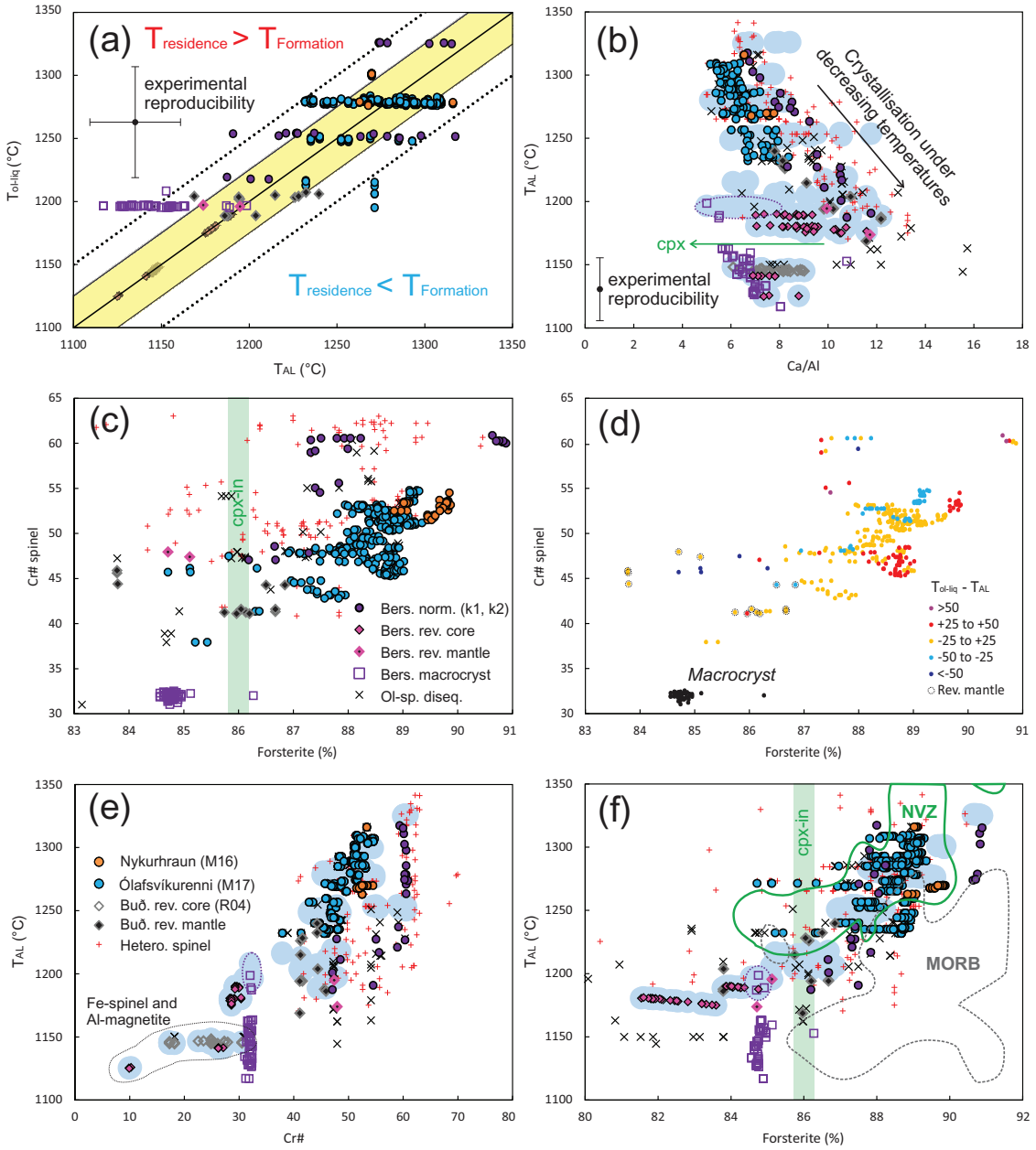

Fig. 10. Temperature–chemistry relationships for olivine and spinel. (a) Comparison of $T_{ol\text{-}liq}$ and T_{AL} for samples suitable for both thermometers. 1:1 line and dotted lines for a ± 50°C interval are shown for reference. Shaded samples on the 1:1 line are far outside the calibration range for T_{AL} (spinel in the cores of reverse zoned olivine) and only have an assigned $T_{ol\text{-}liq}$. Blue shaded fields in (b), (e) and (f) are the fields for olivine-liquid temperatures, samples outside the T_{AL} calibration range (spinel in evolved cores) consequentially correspond exactly with the shaded areas. (b) The temperature-sensitive parameter Ca/Al in olivine plotted against temperature. The data defines a cooling trend (the compatibility of Al in olivine decreases faster than that of Ca with decreasing temperature; De Hoog *et al.*, 2010) with a horizontal offset probably caused by clinopyroxene fractionation, which forms a sink for Ca in the magmatic system (also see Rasmussen *et al.*, 2020). (c) Detail of Fig. 6c, d. Same parameters as (c) but with the samples colour-coded for the difference between $T_{ol\text{-}liq}$ and T_{AL}. (e) Temperatures compared to Cr# spinel. (f) Temperatures against Fo content in olivine. Reference fields with the temperatures for the Northern Volcanic zone (extends to >1350°C) by Matthews *et al.* (2016) and MORB by Coogan *et al.* (2014). Dotted purple ellipsoids encircle $T_{ol\text{-}liq}$ for the core of the olivine macrocryst.

spinel that is mostly surrounded by olivine and a heterogeneous spinel enclosed by melt are visible (Figs 2p and 9a). Al-chromite that is mostly enclosed by olivine (Fig. 9b) has slightly varying compositions, mainly between a more Cr-rich core and a more Al-rich mantle and rim, Mg# increases from the core towards the rim. A second Al-chromite (Fig. 9c) has widely varying compositions and a recrystallized finer grained Cr-spinel aggregate in the surrounding glass. Increasing Fe^{3+} is counterbalanced by decreasing Cr and Al except in the centre of the spinel grain (where two former grains appear to be joined) and the recrystallized spinel where both Al and Fe^{3+} increase at the expense of Cr, probably indicating crystallization from late-stage melt.

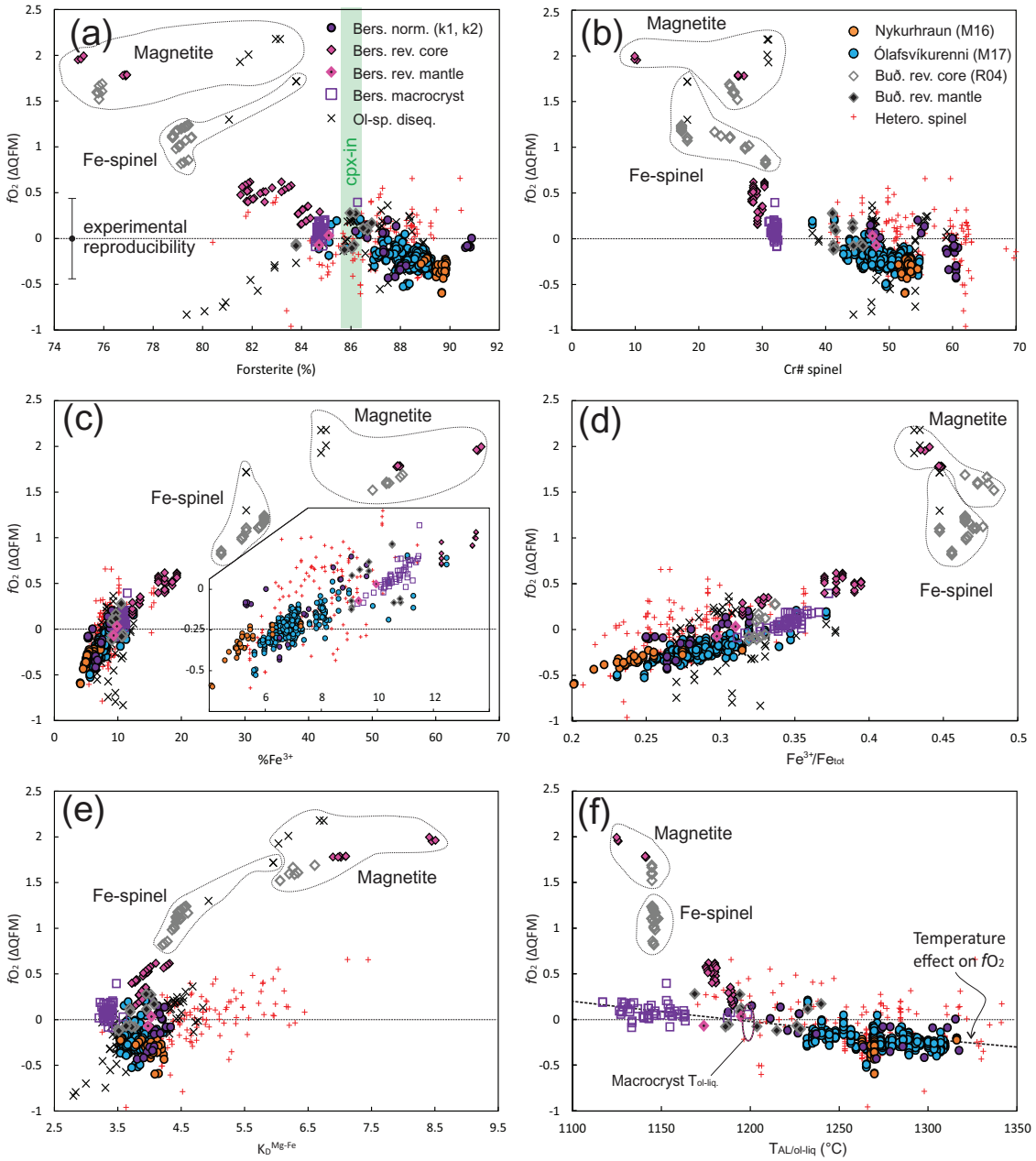

Fig. 11. fO_2 compared to compositional parameters and temperatures. (a) fO_2 compared to forsterite content in olivine. fO_2 gradually increases with decreasing Fo. A similar trend can be observed with Cr# in (b), with the exception that Cr# is separated in more discrete values rather than a continuous range. The relationship with Cr# for Fe-spinel and Al-magnetite is obscured due to their high Fe^{3+} content. The effect of spinel heterogeneity and olivine–spinel disequilibrium on fO_2 is visible in (c) with the disequilibrium pairs having a strong effect and heterogeneous spinel mainly leading to discrepancies in $K_D^{Mg\text{-}Fe}$ and a slight systematic offset to higher fO_2. In (f) fO_2 gradually increases with decreasing T. The trend is broken for the lowest temperature samples that have a wide variation of fO_2 at similar T, broadly around 1150°C. T_{AL} are plotted except for spinel in evolved cores of reverse zoned olivine for which $T_{ol\text{-}liq}$ is used. The dotted line in (f) shows the isolated effect of temperature on fO_2 at fixed spinel and olivine compositions and fixed pressure. The appropriate fO_2 for $T_{ol\text{-}liq}$ for the olivine macrocryst is also indicated.

The outermost rim of the Al-chromite has a sharp elevation in Mg#, mimicking the elevated Fo content of the outermost rim of the associated olivine (Fig. 2o). More subtle heterogeneity results in a high between olivine and spinel caused by low spinel Mg# due to equilibration with melt rather than surrounding olivine, amounting to an overestimation of fO_2. Further, heterogeneous spinel shows a rise in $\%Fe^{3+}$ compared to Fe^{3+}/Fe_{tot} (Supplementary Fig. 1). This is probably due to late-stage oxidation by the melt during and after eruption, as also seen in some spinel from peridotites in contact with the carrier melt (Roeder, 1994). In addition, Fe^{2+} in spinel can potentially oxidize to Fe^{3+}, breaking spinel stoichiometry (Bosi *et al.*, 2004), this would result in inaccurate Fe^{2+}/Fe^{3+} calculation. Either of these interpretations disqualify heterogeneous spinel for accurate

Table 1: Summary of chemical properties, temperature and fO_2 for spinel in different olivine types and localities. fO_2 is calculated at 0.7 GPa for normal zoned olivine and at 0.5 GPa for the other olivine types

Summary of equilibrium assemblages										
Olivine type	Location	Spinel type	Forsterite (%)	Cr# spinel	Mg# spinel	% TiO_2 spinel	% Fe^{3+} spinel	T_{AL} (°C)	$T_{ol\text{-}liq}$ (°C)	$\Delta \log fO_2$ (QFM)
normal zoned	Ólafsvíkurenni	Al-chromite, Cr-spinel	84.7–89.4	37.9–54.8	59.5–69.5	0.6–1.5	5.6–12.5	1232–1309	1195–1284	−0.5–+0.2
normal zoned	Nykurhraun	Al-chromite	88.8–89.9	51.5–54.5	67.2–69.2	0.5	4.1–7.3	1263–1316	1276–1301	−0.6–−0.2
normal zoned	Berserkjahraun	Al-chromite, Cr-spinel	86.2–90.9	47.1–60.9	60.2–70.0	0.6–1.2	5.3–9.6	1187–1317	1195–1284	−0.4–+0.2
Macrocryst	Berserkjahraun	Cr-spinel	84.6–85.1*	31.0–32.5	60.4–62.6*	1.5–1.7	9.3–11.5	1117–1199	1195–1208	−0.1–+0.4
Mantle	Berserkjahraun	Cr-spinel	84.7–85.1	47.4–47.9	57.6–58.0	1.1	9.3–10.0	1174–1195	1196–1197	0
Mantle	Búðahraun	Cr-spinel	83.8–86.8	41.1–45.9	57.2–63.3	1.1–1.2	9.1–10.8	1169–1240	1189–1207	−0.1–+0.3
Evolved core	Berserkjahraun	Cr-spinel	81.5–84.7	28.3–30.4	50.1–57.4	3.8–5.8	12.3–19.3	n.a.	1175–1190	+0.2–+0.6
Evolved core	Búðahraun	Fe-spinel	78.8–79.6	17.3–30.5	43.0–45.8	3.3–6.6	26.3–33.1	n.a.	1144–1148	+0.8–+1.2
Evolved core	Berserkjahraun	Al-magnetite	75.0 -76.9	9.9–27.1	24.1–30.5	12.2–14.7	53.9–67.2	n.a.	1125–1141	+1.8–+2.0
Evolved core	Búðahraun	Al-magnetite	75.7–75.9	24.8–26.1	30.1–31.8	8.8–11.2	50.1–54.8	n.a.	1145	+1.5–+1.7

*excludes rim with $Fo_{86.3}$ and spinel Mg# 63.7
n.a.: not applicable

estimation of the formation temperature and fO_2 conditions.

The olivine–spinel T-fO_2 record

A complete spectrum of olivine types with spinel inclusions is only available from Berserkjahraun, but the data from other locations follow similar thermal, compositional and fO_2 trends providing a general framework. Ólafsvíkurenni and Nykurhraun contain larger normal zoned olivine that is less affected by diffusion and provide a valuable supplement to the primitive portion of the Berserkjahraun dataset. The most important compositional parameters, temperatures and fO_2 for different groups of olivine–spinel pairs are summarized in Table 1 and briefly discussed here. T_{AL} for normal zoned olivine (averaged for the high-current olivine analyses around each spinel for M16 and M17) broadly overlap for Ólafsvíkurenni and Berserkjahraun and has a limited range for Nykurhraun. Reverse zoned rims in Berserkjahraun and Búðahraun have temperatures and oxygen fugacities overlapping with normal zoned olivine with similar Fo content. The olivine macrocryst (Berserkjahraun) and spinel inclusions have lower $K_D^{Mg\text{-}Fe}$ than those in normal zoned olivine, but consistent with their low Cr# (Fig. 6d). With the exception of three spinels, the T_{AL} tightly cluster (Fig. 10) and are distinctly cooler than the temperatures recorded by normal zoned olivines and also significantly cooler than the corresponding $T_{ol\text{-}liq}$. The evolved composition of olivine and spinel may be problematic for T_{AL} and, even though Fe^{3+} is not particularly high, $T_{ol\text{-}liq}$ may be more robust estimate in this case. Both are shown in figures where relevant. The overall fO_2 for spinel in the olivine types with $Fo_{84.5–90.9}$ correlates negatively with Fo content, spinel Cr#, spinel Mg# and temperature but positively with Fe^{3+} (Fig. 11, Supplementary Fig. 1). These trends are interpreted to trace the evolving and cooling parental basaltic melt system.

The cores of reversel zoned olivine contain Cr-spinel (Berserkjahraun; K1/K2), Fe-spinel (Búðahraun; RO4) and Al-magnetite (Berserkjahraun and Búðahraun). Cr-spinel is observed in the diffuse boundary between evolved core and higher Fo mantle, while Fe-spinel and Al-magnetite are found in homogenous olivine cores. $K_D^{Mg\text{-}Fe}$ equilibrium ranges based on Cr-spinel are not appropriate for these spinel types ($K_D^{Mg\text{-}Fe}$ of 4.2–4.6 for Fe-spinel and 6.1–8.5 for Al-magnetite) and equilibrium is assumed based on the observation that homogeneous spinels are surrounded by homogeneous olivine. The lack of $T_{ol\text{-}liq}$ change in the cores of reverse zoned olivines over a large range of olivine and spinel chemistry and fO_2 is a major difference to spinel in more primitive olivine. The compositions of spinel in reverse zoned mantles and in the olivine macrocryst mark a turning point in evolution of the magmatic system where the prevailing effects of gradual cooling are replaced with chemical and fO_2 change over a limited range in temperature (Fig. 11).

Snæfellsnes magmatic systems

Context

Previous studies have unravelled complex multi-tiered crustal magma storage zones at Berserkjahraun, Búðahraun (Kahl *et al.*, submitted), Vatnafell (Burney *et al.*, 2020) and Snæfellsjökull (Kokfelt *et al.*, 2009). The first two studies focus on several geothermometers and clinopyroxene geobarometry to establish the temperature and pressure conditions for olivine–spinel-clinopyroxene-plagioclase fractionating magmas. Although the three eruptions occurred in different parts of the peninsula at different times, the phenocryst populations are similar. These authors identified at least two tiers of crustal magma storage and modification for each locality; one in the mid-upper crust and one in the lowermost crust. The temperature and fO_2 of clinopyroxene-fractionating crustal magma systems is recorded by spinel in reverse zoned olivines and the macrocryst. However, the maximum pressures and temperatures recorded by clinopyroxene-melt equilibrium in the lowermost crust correspond to $\sim Fo_{86}$ olivine (see discussion). Therefore, the normal zoned olivine–spinel pairs chart a third tier of magma storage and melt evolution preceding clinopyroxene crystallization, probably at and/or below Moho depth.

Normal zoned olivine in primitive melts

The compositions of normal zoned olivine–spinel pairs from Berserkjahraun, Ólafsvíkurenni and Nykurhraun provide a mostly continuous data set (Fig. 11). An exception is olivine above Fo_{90}, which does occur in all three locations (Rasmussen *et al.*, 2020; Kahl *et al.*, submitted; this study), but we found only two olivines from Berserkjahraun with spinel inclusions to be that primitive. The normal zoned olivines with $Fo_{84.7–90.9}$ crystallized over a wide range of melt compositions (Figs 4, 6, 10, 11) and temperatures (T_{AL} 1187–1317°C). They appear to have a relatively straightforward chemistry (Fig. 3) and reflect steadily rising fO_2 with melt evolution (Fig. 11) controlled by decreasing temperatures (Fig. 11f). However, the relationship with spinel compositions is more complex. Spinel Mg#, $\%Fe^{3+}$ and Fe^{3+}/Fe_{tot} correlate well with Fo (Fig. 6b, e) and follow the major element composition of olivine equilibrated with a melt with increasing Fe^{3+} and Fe^{2+}. Like Fo content, the Cr# in spinel should trace melt evolution with Cr being a more compatible element than Al. However, spinel Cr# and TiO_2 are only very loosely correlated with Fo (Figs 6c, f and 10c). This may in part be explained by the possibility that spinel formed in more primitive melt before being incorporated in olivine (as an antecryst). In this scenario, olivine Fo content and spinel Cr# reflect different parental melt compositions (Mg# in spinel rapidly adjusts to the surrounding olivine Fo content) and T_{AL} and $T_{ol\text{-}liq}$ would both record the formation temperature of olivine trapping the spinel. A good example is spinel in reverse zoned mantles. These spinels generally have high Cr# for their respective

surrounding olivine Fo content and mostly similar T_{AL} and $T_{ol\text{-}liq}$ (Fig. 10c, d). The contrary is true for the low-Fo regions in normal zoned olivine, which also contain spinel with high Cr# (Fig. 10c, d) but have $T_{AL} \gg T_{ol\text{-}liq}$ (Fig. 10a, d). This phenomenon is probably an effect of diffusive lowering of the olivine Fo content (effectively lowering the $T_{ol\text{-}liq}$ that relies on Mg-Fe^{2+} equilibrated melt) around the spinel, leaving Al in olivine and Cr# in spinel intact (no alteration of T_{AL}). Comparing $T_{ol\text{-}liq}$ (sensitive to diffusive change of Fo content of olivine) and T_{AL} (insensitive to diffusion) differences (Fig. 10a) with spinel and olivine chemistry (Fig 10d) reveals that thermally equilibrated pairs concentrate around a positively correlating trend between Fo in olivine and Cr# in spinel, which probably reflects the chemistry of an evolving and cooling melt system. Spinels with a relatively high Cr# compared to their surrounding olivine Fo content are usually either in thermal equilibrium (spinel antecryst captured by growing olivine) and/or or affected by lowering of olivine Fo content through diffusion, resulting in $T_{ol\text{-}liq} < T_{AL}$. Primitive olivine cores containing spinel with relatively low Cr# from Nykurhraun and Ólafsvíkurenni have $T_{ol\text{-}liq}$ that consistently exceed T_{AL} by >25°C (Fig. 10d). Provided the temperature calculations are accurate, this implies that the olivine and spinel pairs formed at their respective T_{AL} followed by the complete diffusive Mg-Fe^{2+} overprinting of the olivine by more primitive and hotter melts. The large range in T_{AL} that are inconsistent with $T_{ol\text{-}liq}$ for Al-chromites from Berserkjahraun presents a complex case that may be explained if primitive spinel (Cr# 60) was captured by olivine over a range of temperatures (Fig. 10e) before olivine being reset to higher $T_{ol\text{-}liq}$. Therefore, melt mixing and magma processing have already occurred while the primitive melts were traversing the mantle or were ponded below the crust. Initial olivine zoning profiles may have been completely annealed and later replaced by normal zoning patterns; the latter being related to short-term crustal residence and ascent. Low spinel Cr# compared to the primitive host olivine Fo content signals that olivine-liquid thermometry can record ambient rather than formation conditions.

Cr-spinel in reverse zoned olivine mantles

The occurrence of spinel in equilibrium with normal zoned olivine effectively ceases when compositions in equilibrium with the most primitive clinopyroxene are reached (~Fo_{86}). The more evolved olivines with ≤Fo_{86} are reverse zoned and include the (slightly reverse zoned) olivine macrocryst. Cr-spinel similar to that in normal zoned olivine can be found in the more primitive olivine mantles ($Fo_{83.8–86.6}$) of reverse zoned olivine (Fig. 4). In terms of temperature and fO_2, the spinels and olivine mantles also follow the general trend of the normal zoned olivines (Figs 10 and 11). Reverse zoned mantles in olivine and Cr-rich Mg#88 clinopyroxene rims record recharge events by primitive melts in the crust (Kahl *et al.*, submitted; this study). The Ca/Al in such olivine mantles suggests that the recharging melts have not been affected by previous clinopyroxene fractionation (Fig. 10b). The reverse zoned olivines therefore probably formed in the lower crustal tier of magma storage (Kahl *et al.*, submitted; Burney *et al.*, 2020) that is replenished by more primitive melts associated with clinopyroxene-free fractionation of primitive olivine and spinel.

Cr-spinel in reverse zoned low-Fo olivine cores

Cr-spinel also occurs in the cores of two reverse zoned $Fo_{81.5–85.1}$ olivines from Berserkjahraun. Even though the Fo contents of one of these cores overlaps with some of the reversezoned mantles in other olivines, the Cr-spinels are different from the types discussed previously. Compared to Cr-spinel in normal zoned olivine and mantles of reverse zoned olivine, they are relatively rich in Al, Ti and Fe^{3+} (Figs 4, 5) and surrounded by olivine with varied to low Ca/Al at a given temperature, suggesting precipitation of clinopyroxene alongside olivine (Fig. 10b). The Cr# (28.3–30.4) of Cr-spinel in cores of reverse zoned olivines has a very narrow range while spinel Ti, Mg# and the olivine Fo content span wide ranges. Diffusive equilibration of spinel with more evolved melt can readily alter Mg, Fe and Ti but Cr and Al less so (see for example the heterogenous spinel in Fig. 11). Therefore, the spinels probably originate as antecrysts that initially crystallized from a more primitive melt but were overprinted by more evolved (Fe and Ti-rich) melt compositions and then incorporated by olivine, implying a dynamic magma mixing environment, probably associated with a crystal mush pile (Thomson & Maclennan 2013; Mutch *et al.*, 2019). The Cr-spinel in reverse zoned olivine cores have compositions at the onset of the spinel Fe-Ti fractionation trend (Roeder, 1994) that follows melt compositions from which olivine, clinopyroxene and plagioclase are extracted. Contrary to the fO_2 of olivine with >Fo_{86} that closely follows temperature effects, the fO_2 calculated from <Fo_{86} olivine-Cr-spinel pairs rises more rapidly over a narrow temperature interval (1175–1190°C, Fig. 11a, d, Supplementary Fig. 1b,c) and appears to be controlled by oxidation related to magmatic processes.

Cr-spinel in an olivine macrocryst/wehrlite

The 40 individual spinels that were analysed in the low Ca/Al olivine macrocryst from Berserkjahraun are extremely homogeneous (Figs 4, 5), and appear to have crystallized from a single melt in spite of competition over Cr with clinopyroxene (Roeder, 1994). This contrasts with the more varied (in terms of Mg# and Ti) Cr-spinel in the cores of reverse zoned olivines. Competition with clinopyroxene but the absence of plagioclase may explain the uniquely Al-rich nature of the Cr-spinel (Fig. 5). In terms of temperature ($T_{ol\text{-}liq}$), fO_2 and composition, the macrocrystic olivine and spinel form a hinging point between the gradual

compositional trends seen in normal zoned olivines and mantles of reverse zoned olivines and the Ti-Fe trend formed by spinel in cores of reverse zoned olivines. Macrocrystic olivine and spinel compositions probably represent crystallization of crystal mushes in the mid-lower crustal magma storage zones (Kahl *et al.*, submitted) at ~QFM and ~1200°C in a relatively quiet magmatic environment.

Al-Fe-Ti spinel and the spinel gap

Fe-spinel and, to a lesser extent, Cr-Ti-bearing Al-magnetite observed in reverse zoned cores of olivines from Búðahraun and Berserkjahraun have rare compositions that fall within the 'spinel gap' (Fig. 4; Roeder, 1994; Barnes & Roeder 2001). The global scarcity of such spinel compositions has previously been explained by the stability of clinopyroxene in more evolved basaltic melts (Roeder, 1994), combined with the limited miscibility between Fe-rich and Al-rich spinel species (Lehmann and Roux 1986; Sack and Ghiorso 1991a; Fig. 12). The presence of Al-rich spinel in the olivine macrocryst, however, indicates that crystallization of Cr-poor spinel alongside clinopyroxene *is* possible. Furthermore, the relatively high olivine-liquid temperatures of the Fe-Al-rich spinels reveal that they formed because the temperatures exceeded those of the immiscibility region (Fig. 12). The Berserkjahraun samples studied here are glassy scoria with spinel-melt textures indicative of very fast cooling (Fig. 2p; Roeder *et al.*, 2001). Rapid cooling of initially hot melts seems to have preserved spinel near the apex of the 'spinel gap'. Oxybarometry for olivine and spinel of these exotic compositions has fair amount of uncertainty because the spinel compositions are outside the calibration range (Nikolaev *et al.*, 2016). Nevertheless, the formation of magnetite requires oxygen fugacities that are several log units higher than the QFM buffer (e.g. Hill & Roeder 1974) and our results appear to be consistent with several compositional trends (Fig. 11a, Supplementary Fig. 1b), suggesting oxygen fugacities $\Delta\log f\mathrm{O}_2$ (QFM) of around +1 (Fe-spinel) and $+1.5 \pm 2$ (Al-magnetite) are not far off. These results imply a further chemical fractionation and oxygenation of the magmatic systems over a limited temperature array (1125–1148°C). These most evolved spinel and olivine compositions probably correspond to storage within the upper-crustal magma storage zones identified by Kahl *et al.* (submitted) and Burney *et al.* (2020).

The Snæfellsnes mantle source

On Snæfellsnes, magma is sourced from a greater average depth than at the actively spreading rift zones due to a thicker lithosphere (Elliott *et al.*, 1991). A substantiated estimate of lithospheric thickness under Snæfellsnes is currently lacking but we assume it to be around 55 km based on the lithosphere under the Westfjords, north of Snæfellsnes (Bjarnason & Schmeling, 2009). The transitional to alkaline magmas

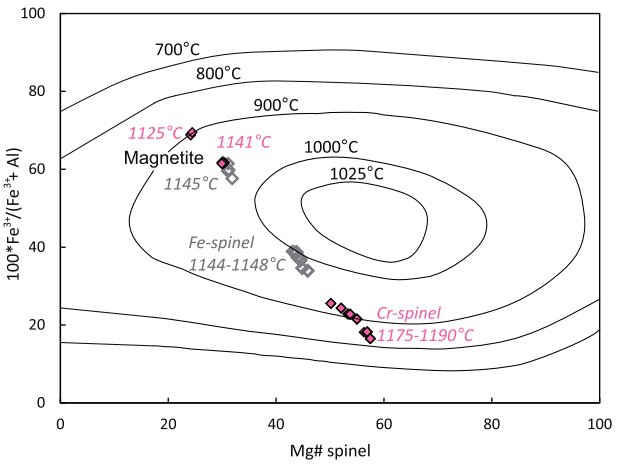

Fig. 12. Fe^{3+}-rich Cr-spinel, Fe-spinel and Al-magnetite with compositions traversing the 'spinel gap' compared to the temperature contours for immiscibility (Sack & Ghiorso 1991b). The grey and pink italic numbers are olivine-liquid temperatures at the textural positions of the spinels, which are consistently above the upper limit for miscibility.

formed in the SNVZ are compositionally distinct from Icelandic rift basalts. They are rich in incompatible trace elements and have isotopic compositions trending towards FOZO or PREMA (Kokfelt *et al.*, 2006; Peate *et al.*, 2010). These properties are best explained by low-degree melting of a chemically heterogeneous mantle, causing fertile and isotopically enriched components to control the resulting bulk magmas (Kokfelt *et al.*, 2006; Koornneef *et al.*, 2012). Petrologically, however, the primitive melts from Snæfellsnes are dominated by an olivine-bearing (peridotitic) source rather than pyroxenite (Nikkola *et al.*, 2019a; Rasmussen *et al.*, 2020; Fig. 3). This is reflected by the most primitive olivines ($>\mathrm{Fo}_{89}$) that have low Ni and high 100 Mn/Fe (Fig. 3) and their spinel inclusions have low TiO_2 and high Al_2O_3 (Fig. 5a), overlapping with the most fertile extent of MORB. Primitive olivines and spinels with $\Delta\log f\mathrm{O}_2$ (QFM) −0.6 to −0.1 are reduced relative to MORB, which has $f\mathrm{O}_2$ around the QFM buffer (Zhang *et al.*, 2018; Berry *et al.*, 2018). However, the envelope of oxygen fugacities with evolving melts containing olivine up to $\sim\mathrm{Fo}_{85}$ (Fig. 11a) can be completely explained by changing temperature conditions (dotted line in Fig. 11f). Therefore, the more primitive Snæfellsnes olivine–spinel pairs are in part more reduced due to elevated crystallization pressures and temperatures (cf. MORB field in Fig. 10f). Normal zoned olivine–spinel pairs with T_{AL} between 1200 and 1250°C, a more representative temperature range for MORB (Coogan *et al.*, 2014: Fig. 10f), have $\Delta\log f\mathrm{O}_2$ (QFM) between −0.3 and 0.0 (Fig. 11f). Under the same melting conditions, the source would in effect be only slightly reducing relative to the MORB source but overlap entirely if the error on the method, or uncertainty surrounding the oxidation state of the MORB source are included. Mildly reducing conditions support the notion of melts that are buffered by peridotite rather than a fertile pyroxenite component beneath Snæfellsnes

(Nikkola *et al.*, 2019a; Rasmussen *et al.*, 2020; Figs 3, 4). Olivine–spinel data from Snæfellsnes contrasts with that from South Iceland (Nikkola *et al.*, 2019a), which is more enriched and overlaps with the OIB field (Kamenetsky *et al.*, 2001; Fig. 5a). South Iceland also appears to be somewhat more oxidized, with the most primitive olivine and spinel recording fO_2 conditions between Δlog fO_2 (QFM) -0.4 ± 1.0. These properties may be related to a more dominant pyroxenite component in the mantle source and emphasizes the subtle but fundamental differences between distinct off-rift magmatic regions in Iceland.

Causes for volcanism

The occurrence of SNVZ volcanism remains somewhat enigmatic but could be enabled by strike-slip faulting (Sigurdsson, 1970). This alone may not be sufficient; a trans-crustal transform fault in South Iceland (SISZ; Fig. 1) is tectonically more active but essentially non-magmatic (e.g. Pedersen *et al.*, 2003; Sinton *et al.*, 2005). The range in temperatures for primitive olivine–spinel pairs support a warm mantle source under Snæfellsnes with crystallization temperatures (T_{AL}) up to ~1315°C. These temperatures overlap with, and exceed, the highest olivine crystallization temperatures for MORB (Coogan *et al.*, 2014) and are overlapping but low compared to Icelandic rift volcanism (Spice *et al.*, 2016; Matthews *et al.*, 2016). It is possible that the horizontal flow of warm asthenosphere away from the plume centre is guided along the main fracture network expressed at the surface, i.e. the rift zones and MIB (Fig. 1) and that elevated mantle temperatures may enable the volcanic activity here. The reliance of volcanism enabled by tectonism explains the isolated and limited magmatic productivity on Snæfellsnes (Kokfelt *et al.*, 2006; 2009; Thordarson and Höskuldsson 2008; Sigmarsson et al., 2008; Peate *et al.*, 2010; Burney *et al.*, 2020). Furthermore, the control of temperature on the oxygen fugacity (Fig. 11f) is an expected feature of decompression, rather than heating controlled mantle melting (Gaetani, 2016), supporting a tectonic control on melt generation in the SNVZ. The limited melt fluxes of Snæfellsnes volcanic systems (Kahl *et al.*, submitted), combined with tectonically controlled pathways in relatively cool crust, probably result in locally distinct magmatic systems. This may explain the variety in crystal populations observed in the different examined magmatic systems as Berserkjahraun, Búðahraun and Vatnafell are all sourced from multiple tiers of crustal magma chambers (Burney *et al.*, 2020; Kahl *et al.*, submitted; this study). In the case of Vatnafell, crustal magma processing accounts for the entire observed range of crystal compositions (clinopyroxene Mg# 72–87 and $Fo_{72\text{-}84}$ olivine; Burney *et al.*, 2020), while Berserkjahraun and Búðahraun also include more primitive olivine with up to Fo_{91} (Kahl *et al.*, submitted; Rasmussen *et al.*, 2020; this study), suggesting crystallization directly from primary mantle-melt aggregates (Albarede, 1992; Putirka *et al.*, 2007; Herzberg, 2011). By contrast, all olivines from Ólafsvíkurenni and Nykurhraun are primitive (also up to Fo_{91}; Rasmussen *et al.*, 2020) and normal zoned, lacking evidence for clinopyroxene co-crystallization and suggesting minimal crustal processing of these lavas. We also find that aggregated lavas at Búðahraun and Berserkjahraun are more oxidized than those from Nykurhaun and Ólafsvíkurenni due to extensive magma plumbing processing. These observations support widely varying temporally and locally controlled magma plumbing systems sourcing volcanism on Snæfellsnes.

CONCLUSIONS

1. The crystallization temperatures and oxygen fugacity of basaltic olivine phenocrysts with included Cr-spinel and Al-chromite can be calculated when homogeneous spinel is completely enclosed by homogeneous olivine. Geologically meaningful results can sometimes be obtained when homogenous spinel is enclosed in mildly zoned olivine and the mineral pair has $K_D^{Mg\text{-}Fe}$ within the range for homogenous spinel in homogeneous olivine. Equilibrium $K_D^{Mg\text{-}Fe}$ for the examined Snæfellsnes olivine–spinel pairs falls between 3.5 and 4.3, which may serve as a rough initial guide for spinel–olivine pairs of similar composition (Cr# 38-61, Fe^{3+}/Fe_{tot} 0.20–0.37 in $Fo_{85\text{-}91}$ olivine). In a similar fashion $K_D^{Mg\text{-}Fe}$ may be assessed based on unzoned spinel in unzoned olivine from other volcanic regions. Olivine paired with heterogeneous spinel or spinel in touch with the melt (glass) is unreliable because spinel partially equilibrates with late-stage melt.
2. Al-chromite and Cr-spinel in normal zoned olivine record the primitive stages of magma fractionation and crystallized from clinopyroxene-free melts. Discrepancies between $T_{ol\text{-}liq}$ (Mg-Fe^{2+} diffusion sensitive) and T_{AL} (diffusion insensitive) suggest that some primitive olivines experienced magma mixing to a degree, overprinting their Fo content. This probably occurred around the base of the crust or in the upper mantle. Temperature (1187–1317°C) gradually cool with decreasing olivine $Fo_{84.7\text{-}90.9}$ and controls an increase in fO_2 (Δlog fO_2 (QFM) -0.6 ± 0.2).
3. The most primitive Cr-spinel representing lower crustal magma storage conditions, occurs in the primitive $Fo_{83.8\text{-}86.8}$ mantles of reverse zoned olivines. These spinels are mostly antecrysts with high Cr# (41.1–47.9) that were captured by olivine and equilibrated in terms of Mg-Fe^{2+}. Their compositions and fO_2 continue trends from normal zoned olivines and represent primitive magma compositions that recharged more fractionated crustal magma storage zones.
4. Rare Cr-spinel antecrysts introduced to more evolved melts are found in the evolved cores of reverse zoned olivines. These are overprinted by

fractionating melt with increasing Ti and Fe before being trapped in $Fo_{81.5\text{-}84.7}$ olivine. These spinels record chemical and fO_2 change in crustal magma chambers over a limited temperature range.

5. A rare olivine macrocryst crystallized alongside clinopyroxene (wehrlite) and has abundant Al-rich homogenous spinel inclusions. This olivine and its spinel inclusions are special because they appear to record closed magma chamber fractional crystallization rather than magma mixing. The homogeneous spinel incorporated in the olivine indicates that Cr-poor spinel can crystallize alongside clinopyroxene. The olivine–spinel pairs record lower crustal crystal mush conditions with fO_2 around the QFM buffer and $T_{ol\text{-}liq}$ of $\sim$1200°C, similar to recharge-related mantles of reverse zoned olivine.
6. The most evolved cores of reverse zoned olivine from Búðahraun and Berserkjahran contain Fe-spinel and Al-magnetite signalling a further increase in Fe, Ti and fO_2 in the melt over a limited temperature interval (1125–1148°C). These compositions are rare for spinel and span the 'spinel gap'. Their preservation is probably related to crystallization in high-temperature magmas and rapid cooling after eruption.
7. Spinel and olivine compositions support tectonically controlled decompression melting of a slightly reduced fertile peridotitic source at elevated mantle temperatures beneath Snæfellsnes. This contrasts with the more oxidized and pyroxenite sourced off-rift magmatism in South Iceland.

ACKNOWLEDGEMENTS

The authors would like to thank Sunna Harðardóttir for sharing unpublished data, Anne Beuk and Rebekka Hlín Rúnarsdóttir for assistance with sample preparation and Sæmundur Ari Halldórsson, Teresa Ubide, Edward Marshall, Rikke Pedersen and Simon Matthews for valuable discussions. Editorial comments from Adam Kent and reviews by Euan Mutch and two anonymous reviewers improved the quality of the paper.

SUPPLEMENTARY DATA

Supplementary data are available at *Journal of Petrology* online.

REFERENCES

Albarede, F. (1992). How deep do common basaltic magmas form and differentiate? *Journal of Geophysical Research* **97**, 10997–11009.

Allan, J. F. (1994). Cr-spinel in depleted basalts from the Lau basin backard: petrogenetic history from Mg-Fe crystal-liquid exchange. In: *Proceedings of the Ocean Drilling Program. Scientific Results*, **135**, pp. 565–583.

Ballhaus, C., Berry, R. F. & Green, D. H. (1991). High pressure experimental calibration of the olivine-orthopyroxene-spinel oxygen geobarometer: implications for the oxidation state of the upper mantle. *Contributions to Mineralogy and Petrology* **107**, 27–40.

Barnes, S. J. & Roeder, P. L. (2001). The range of spinel compositions in terrestrial mafic and ultramafic rocks. *Journal of Petrology* **42**, 2279–2302.

Berry, A. J., Stewart, G. A., O'Neill, H. S. C., Mallmann, G. & Mosselmans, J. F. W. (2018). A re-assessment of the oxidation state of iron in MORB glasses. *Earth and Planetary Science Letters* **483**, 114–123.

Bjarnason, I. T. & Schmeling, H. (2009). The lithosphere and asthenosphere of the Iceland hotspot from surface waves. *Geophysical Journal International* **178**, 394–418.

Blundy, J., Melekhova, E., Ziberna, L., Humphreys, M. C., Cerantola, V., Brooker, R. A., McCammon, C. A., Pichavant, M. & Ulmer, P. (2020). Effect of redox on Fe–Mg–Mn exchange between olivine and melt and an oxybarometer for basalts. *Contributions to Mineralogy and Petrology* **175**, 1–32.

Bosi, F., Andreozzi, G. B., Ferrini, V. & Lucchesi, S. (2004). Behavior of cation vacancy in kenotetrahedral Cr-spinels from Albanian eastern belt ophiolites. *American Mineralogist* **89**, 1367–1373.

Breddam, K. (2002). Kistufell: primitive melt from the Iceland mantle plume. *Journal of Petrology* **43**, 345–373.

Brounce, M., Stolper, E. & Eiler, J. (2017). Redox variations in Mauna Kea lavas, the oxygen fugacity of the Hawaiian plume, and the role of volcanic gases in Earth's oxygenation. *Proceedings of the National Academy of Sciences* **114**, 8997–9002.

Burney, D., Peate, D. W., Riishuus, M. S. & Ukstins, I. A. (2020). Reconstructing the plumbing system of an off-rift primitive alkaline tuya (Vatnafell, Iceland) using geothermobarometry and CSDs. *Journal of Volcanology and Geothermal Research* **339**, 106914.

Burnham, A. D. & Berry, A. J. (2012). An experimental study of trace element partitioning between zircon and melt as a function of oxygen fugacity. *Geochimica et Cosmochimica Acta* **95**, 196–212.

Burnham, A. D., Mallmann, G. & Fonseca, R. O. (2020). Mineral-melt partitioning of redox-sensitive elements. *Journal of Earth and Space Science Open Archive*, doi: 10.1002/essoar.10503118.1.

Canil, D., O'Neill, H. S. C., Pearson, D. G., Rudnick, R. L., McDonough, W. F. & Carswell, D. A. (1994). Ferric iron in peridotites and mantle oxidation states. *Earth and Planetary Science Letters* **123**, 205–220.

Coogan, L. A., Saunders, A. D. & Wilson, R. N. (2014). Aluminum-in-olivine thermometry of primitive basalts: evidence of an anomalously hot mantle source for large igneous provinces. *Chemical Geology* **368**, 1–10.

Cherniak, D. J. & Liang, Y. (2014). Titanium diffusion in olivine. *Geochimica et Cosmochimica Acta* **147**, 43–57.

De Hoog, J. C., Gall, L. & Cornell, D. H. (2010). Trace-element geochemistry of mantle olivine and application to mantle petrogenesis and geothermobarometry. *Chemical Geology* **270**, 196–215.

Debaille, V., Trønnes, R. G., Brandon, A. D., Waight, T. E., Graham, D. W. & Lee, C. T. A. (2009). Primitive off-rift basalts from Iceland and Jan Mayen: Os-isotopic evidence for a mantle source containing enriched subcontinental lithosphere. *Geochimica et Cosmochimica Acta* **73**, 3423–3449.

Dohmen, R. & Chakraborty, S. (2007). Fe–Mg diffusion in olivine II: point defect chemistry, change of diffusion mechanisms and a model for calculation of diffusion coefficients in natural olivine. *Physics and Chemistry of Minerals* **34**, 409–430.

Elliott, T. R., Hawkesworth, C. J. & Grönvold, K. (1991). Dynamic melting of the Iceland plume. *Nature* **351**, 201–206.

Feig, S. T., Koepke, J. & Snow, J. E. (2010). Effect of oxygen fugacity and water on phase equilibria of a hydrous tholeiitic basalt. *Contributions to Mineralogy and Petrology* **160**, 551–568.

Gaetani, G. A. (2016). The behavior of $Fe^{3+}/\sum$ Fe during partial melting of spinel lherzolite. *Geochimica et Cosmochimica Acta* **185**, 64–77.

Hardarson, B. S., Fitton, J. G., Ellam, R. M. & Pringle, M. S. (1997). Rift relocation—a geochemical and geochronological investigation of a palaeo-rift in northwest Iceland. *Earth and Planetary Science Letters* **153**, 181–196.

Harðardóttir, S. (2020). Spatial distribution and geochemical characterization of Icelandic mantle end-members. Master's thesis, Faculty of Earth Sciences, University of Iceland, p. 84.

Harðarson, B. S. (1993). Alkalic rocks in Iceland with special reference to the Snæfellsjökull volcanic system. Unpublished Ph.D. thesis, University of Edinburgh.

Hartley, M. E., Shorttle, O., Maclennan, J., Moussallam, Y. & Edmonds, M. (2017). Olivine-hosted melt inclusions as an archive of redox heterogeneity in magmatic systems. *Earth and Planetary Science Letters* **479**, 192–205.

Helgason, Ö., Óskarsson, N. & Sigvaldason, G. E. (1992). Oxygen fugacity stratification of a magma chamber revealed by Mössbauer spectroscopy: evidence from the 1875 Askja eruption. *Hyperfine Interactions* **70**, 989–992.

Herzberg, C. (2011). Basalts as temperature probes of Earth's mantle. *Geology* **39**, 1179–1180.

Hill, R. & Roeder, P. (1974). The crystallization of spinel from basaltic liquid as a function of oxygen fugacity. *The Journal of Geology* **82**, 709–729.

Howarth, G. H. & Harris, C. (2017). Discriminating between pyroxenite and peridotite sources for continental flood basalts (CFB) in southern Africa using olivine chemistry. *Earth and Planetary Science Letters* **475**, 143–151.

Irvine, T. N. (1965). Chromian spinel as a petrogenetic indicator: Part 1. Theory. *Canadian Journal of Earth Sciences* **2**, 648–672.

Irvine, T. N. (1967). Chromian spinel as a petrogenetic indicator: Part 2. Petrologic applications. *Canadian Journal of Earth Sciences* **4**, 71–103.

Jakobsson, S. P. (1972). Chemistry and distribution pattern of recent basaltic rocks in Iceland. *Lithos* **5**, 365–338.

Jarosewich, E. (2002). Smithsonian microbeam standards. *Journal of Research of the National Institute of Standards and Technology* **107**, 681–685.

Jóhannesson, H. (1980). Evolution of rift zones in western Iceland (in Icelandic). *Natturufraedingurinn* **50**, 13–31.

Jóhannesson, H. (1994). *Geological Map of Iceland, Sheet 2, West-Iceland,* 2nd edn. Reykjavik: Icelandic Museum of Natural History and Iceland Geodetic Survey.

Jollands, M. C., Hermann, J., O'Neill, H. S. C., Spandler, C. & Padrón-Navarta, J. A. (2016). Diffusion of Ti and some divalent cations in olivine as a function of temperature, oxygen fugacity, chemical potentials and crystal orientation. *Journal of Petrology* **57**, 1983–2010.

Kamenetsky, V. S., Crawford, A. J. & Meffre, S. (2001). Factors controlling chemistry of magmatic spinel: an empirical study of associated olivine, Cr-spinel and melt inclusions from primitive rocks. *Journal of Petrology* **42**, 655–671.

Kahl, M., Bali, E., Guðfinnsson, G. H., Neave, D. A., Ubide, T., van der Meer, Q. H. A. & Matthews, S. (submitted) Conditions and dynamics of magma storage in the Snæfellsnes volcanic zone, Western Iceland: insights from the Búðahraun and Berserkjahraun eruptions. *Journal of Petrology*

Kolzenburg, S., Di Genova, D., Giordano, D., Hess, K. U. & Dingwell, D. B. (2018). The effect of oxygen fugacity on the rheological evolution of crystallizing basaltic melts. *Earth and Planetary Science Letters* **487**, 21–32.

Kokfelt, T. F., Hoernle, K., Lundstrom, C., Hauff, F. & van den Bogaard, C. (2009). Time-scales for magmatic differentiation at the Snaefellsjökull central volcano, western Iceland: constraints from U–Th–Pa–Ra disequilibria in post-glacial lavas. *Geochimica et Cosmochimica Acta* **73**, 1120–1144.

Kokfelt, T. F., Hoernle, K. A. J., Hauff, F., Fiebig, J., Werner, R. & Garbe-Schönberg, D. (2006). Combined trace element and Pb-Nd–Sr-O isotope evidence for recycled oceanic crust (upper and lower) in the Iceland mantle plume. *Journal of Petrology* **47**, 1705–1749.

Koornneef, J. M., Stracke, A., Bourdon, B., Meier, M. A., Jochum, K. P., Stoll, B. & Grönvold, K. (2012). Melting of a two-component source beneath Iceland. *Journal of Petrology* **53**, 127–157.

Kress, V. C. & Carmichael, I. S. (1991). The compressibility of silicate liquids containing Fe_2O_3 and the effect of composition, temperature, oxygen fugacity and pressure on their redox states. *Contributions to Mineralogy and Petrology* **108**, 82–92.

Kumar, P., Kind, R., Priestley, K. & Dahl-Jensen, T. (2007). Crustal structure of Iceland and Greenland from receiver function studies. *Journal of Geophysical Research* **112**, B03301.

Lehmann, J. & Roux, J. (1986). Experimental and theoretical study of $(Fe^{2+}$, Mg)(Al, $Fe^{3+})$ $2O_4$ spinels: activity-composition relationships, miscibility gaps, vacancy contents. *Geochimica et Cosmochimica Acta* **50**, 1765–1783.

Loucks, R. R. (1996). A precise olivine-augite Mg-Fe-exchange geothermometer. *Contributions to Mineralogy and Petrology* **125**, 140–150.

Mallmann, G. & O'Neill, H. S. C. (2009). The crystal/melt partitioning of V during mantle melting as a function of oxygen fugacity compared with some other elements (Al, P, Ca, Sc, Ti, Cr, Fe, Ga, Y, Zr and Nb). *Journal of Petrology* **50**, 1765–1794.

Martin, E., Paquette, J. L., Bosse, V., Ruffet, G., Tiepolo, M. & Sigmarsson, O. (2011). Geodynamics of rift–plume interaction in Iceland as constrained by new $^{40}Ar/^{39}Ar$ and in situ U–Pb zircon ages. *Earth and Planetary Science Letters* **311**, 28–38.

Matthews, S., Shorttle, O. & Maclennan, J. (2016). The temperature of the Icelandic mantle from olivine-spinel aluminum exchange thermometry. *Geochemistry, Geophysics, Geosystems* **17**, 4725–4752.

Matthews, S., Wong, K., Shorttle, O., Edmonds, M. & Maclennan, J. (2020). Do olivine crystallization temperatures faithfully record mantle temperature variability? Geochemistry, Geophysics, Geosystems

Mutch, E. J., Maclennan, J., Holland, T. J. & Buisman, I. (2019). Millennial storage of near-Moho magma. *Science (New York, N.Y.)* **365**, 260–264.

Mutch, E. J. F., Maclennan, J., Shorttle, O., Rudge, J. F. & Neave, D. A. (2021). DFENS: diffusion chronometry using finite elements and nested sampling. *Geochemistry, Geophysics, Geosystems* **22**, doi:10.1029/2020GC009303.

Nash, W. M., Smythe, D. J. & Wood, B. J. (2019). Compositional and temperature effects on sulfur speciation and solubility in silicate melts. *Earth and Planetary Science Letters* **507**, 187–198.

Nikkola, P., Bali, E., Kahl, M., van der Meer, Q. H., Rämö, O. T., Guðfinnsson, G. H. & Thordarson, T. (2019a). Mid-crustal storage and crystallization of Eyjafjallajökull ankaramites, South Iceland. *Jökull* **69**, 77–96.

Nikkola, P., Guðfinnsson, G. H., Bali, E., Rämö, O. T., Fusswinkel, T. & Thordarson, T. (2019b). Signature of deep mantle melting in South Iceland olivine. *Contributions to Mineralogy and Petrology* **174**, 43.

Nikolaev, G. S., Ariskin, A. A., Barmina, G. S., Nazarov, M. A. & Almeev, R. R. (2016). Test of the Ballhaus–Berry–Green Ol–Opx–Sp oxybarometer and calibration of a new equation for estimating the redox state of melts saturated with olivine and spinel. *Geochemistry International* **54**, 301–320.

Novella, D., Maclennan, J., Shorttle, O., Prytulak, J. & Murton, B. J. (2020). A multi-proxy investigation of mantle oxygen fugacity along the Reykjanes Ridge. *Earth and Planetary Science Letters* **531**, 115973.

Óskarsson, N., Helgason, Ö. & Steinthórsson, S. (1994). Oxidation state of iron in mantle-derived magmas of the Icelandic rift zone. *Hyperfine Interactions* **91**, 733–737.

Peate, D. W., Breddam, K., Baker, J. A., Kurz, M. D., Barker, A. K., Prestvik, T., Grassineau, N. & Skovgaard, A. C. (2010). Compositional characteristics and spatial distribution of enriched Icelandic mantle components. *Journal of Petrology,* **51**, 1447–1475.

Pedersen, R., Jónsson, S., Árnadóttir, T., Sigmundsson, F., & Feigl, K. L., (2003). & Fault slip distribution of two, J. (2000). MW6. 5 earthquakes in South Iceland estimated from joint inversion of InSAR and GPS measurements. *Earth and Planetary Science Letters* **213**, 487–502.

Petry, C., Chakraborty, S. & Palme, H. (2004). Experimental determination of Ni diffusion coefficients in olivine and their dependence on temperature, composition, oxygen fugacity, and crystallographic orientation. *Geochimica et Cosmochimica Acta* **68**, 4179–4188.

Putirka, K. D. (2008). Thermometers and barometers for volcanic systems. *Reviews in Mineralogy and Geochemistry* **69**, 61–120.

Putirka, K. D., Perfit, M., Ryerson, F. J. & Jackson, M. G. (2007). Ambient and excess mantle temperatures, olivine thermometry, and active vs. passive upwelling. *Chemical Geology* **241**, 177–206.

Rasmussen, M. B., Halldórsson, S. A., Gibson, S. A. & Guðfinnsson, G. H. (2020). Olivine chemistry reveals compositional source heterogeneities within a tilted mantle plume beneath Iceland. *Earth and Planetary Science Letters* **531**, 116008.

Roeder, P. L. & Emslie, R. (1970). Olivine-liquid equilibrium. *Contributions to Mineralogy and Petrology* **29**, 275–289.

Roeder, P. L. & Campbell, I. H. (1985). The effect of postcumulus reactions on composition of chrome-spinels from the Jimberlana intrusion. *Journal of Petrology* **26**, 763–786.

Roeder, P. L. & Reynolds, I. (1991). Crystallization of chromite and chromium solubility in basaltic melts. *Journal of Petrology* **32**, 909–934.

Roeder, P. L. (1994). Chromite; from the fiery rain of chondrules to the Kilauea Iki lava lake. *The Canadian Mineralogist* **32**, 729–746.

Roeder, P. L., Poustovetov, A. & Oskarsson, N. (2001). Growth forms and composition of chromian spinel in MORB magma: diffusion-controlled crystallization of chromian spinel. *The Canadian Mineralogist* **39**, 397–416.

Roeder, P. L., Thornber, C., Poustovetov, A. & Grant, A. (2003). Morphology and composition of spinel in Pu'u'O'o lava (1996–1998), Kilauea volcano, Hawaii. *Journal of Volcanology and Geothermal Research* **123**, 245–265.

Rychert, C. A., Harmon, N. & Armitage, J. J. (2018). Seismic imaging of thickened lithosphere resulting from plume pulsing beneath Iceland. *Geochemistry, Geophysics, Geosystems* **196**, 1789–1799.

Sack, R. O. & Ghiorso, M. S. (1991a). Chromian spinels as petrogenetic indicators: thermodynamics and petrological applications. *American Mineralogist* **76**, 827–847.

Sack, R. O. & Ghiorso, M. S. (1991b). An internally consistent model for the thermodynamic properties of Fe−Mg-titanomagnetite-aluminate spinels. *Contributions to Mineralogy and Petrology* **106**, 474–505.

Schipper, C. I. & Moussallam, Y. (2017). Temporal redox variation in basaltic tephra from Surtsey volcano (Iceland). *Bulletin of Volcanology* **79**, 71.

Scowen, P. A. H., Roeder, P. L. & Helz, R. T. (1991). Reequilibration of chromite within Kilauea Iki lava lake, Hawaii. *Contributions to Mineralogy and Petrology* **107**, 8–20.

Shorttle, O., Moussallam, Y., Hartley, M. E., Maclennan, J., Edmonds, M. & Murton, B. J. (2015). Fe-XANES analyses of Reykjanes Ridge basalts: Implications for oceanic crust's role in the solid Earth oxygen cycle. *Earth and Planetary Science Letters*, **427**, 272–285.

Sigmarsson, O., Maclennan, J. & Carpentier, M. (2008). Geochemistry of igneous rocks in Iceland: a review. *Jökull* **58**, 139–161.

Sigurdsson, H. (1970). Structural origin and plate tectonics of the Snaefellsnes volcanic zone, Western Iceland. *Earth and Planetary Science Letters* **10**, 129–113.

Sinton, J., Grönvold, K. & Saemundsson, K. (2005). Postglacial eruptive history of the western volcanic zone, Iceland. *Geochemistry, Geophysics, Geosystems* **6**.

Sobolev, A. V., Hofmann, A. W., Kuzmin, D. V., Yaxley, G. M., Arndt, N. T., Chung, S. L. & Teklay, M. (2007). The amount of recycled crust in sources of mantle-derived melts. *Science*, **316**, 412–417.

Spandler, C. & O'Neill, H. S. C. (2010). Diffusion and partition coefficients of minor and trace elements in San Carlos olivine at 1,300°C with some geochemical implications. *Contributions to Mineralogy and Petrology* **159**, 791–818.

Spice, H. E., Fitton, J. G. & Kirstein, L. A. (2016). Temperature fluctuation of the Iceland mantle plume through time. *Geochemistry, Geophysics, Geosystems* **17**, 243–254.

Sæmundsson, K. (1979). Outline of the geology of Iceland. *Jökull* **29**, 7–28.

Thomson, A. & Maclennan, J. (2013). The distribution of olivine compositions in Icelandic basalts and picrites. *Journal of Petrology* **54**, 745–768.

Thordarson, T. & Höskuldsson, Á. (2008). Postglacial volcanism in Iceland. *Jökull* **58**, 197–228.

Thy, P. (1983). Spinel minerals in transitional and alkali basaltic glasses from Iceland. *Contributions to Mineralogy and Petrology* **83**, 141–149.

Thordarson, T. & Larsen, G. (2007). Volcanism in Iceland in historical time: Volcano types, eruption styles and eruptive history. *Journal of Geodynamics* **43**, 118–152.

Toplis, M. J. & Carroll, M. R. (1995). An experimental study of the influence of oxygen fugacity on Fe-Ti oxide stability, phase relations, and mineral–melt equilibria in ferro-basaltic systems. *Journal of Petrology* **36**, 1137–1170.

van der Meer, Q. H., Scott, J. M., Serre, S. H., Whitehouse, M. J., Kristoffersen, M., Le Roux, P. J. & Pope, E. C. (2019). Low-δ^{18}O zircon xenocrysts in alkaline basalts; a window into the complex carbonatite-metasomatic history of the Zealandia lithospheric mantle. *Geochimica et Cosmochimica Acta* **254**, 21–39.

Vogt, K., Dohmen, R. & Chakraborty, S. (2015). Fe-Mg diffusion in spinel: new experimental data and a point defect model. *American Mineralogist* **100**, 2112–2122.

Wang, Z., Coogan, L. A. & Canil, D. (2008). Experimental calibration of aluminum partitioning between olivine and spinel as a geothermometer. *American Mineralogist* **93**, 1142–1147.

Zhang, H. L., Cottrell, E., Solheid, P. A., Kelley, K. A. & Hirschmann, M. M. (2018). Determination of $Fe^{3+}/\Sigma Fe$ of XANES basaltic glass standards by Mössbauer spectroscopy and its application to the oxidation state of iron in MORB. *Chemical Geology* **479**, 166–175.